Shifted Linear Interpolation for Images

Nasrin Dorreh

Submitted to
Institute of Graduate Studies and Research
in partial fulfillment of the requirements for the Degree of

Master of Science
in
Electrical and Electronic Engineering

Eastern Mediterranean University
January 2014
Gazimağusa, North Cyprus

Approval of the Institute of Graduate Studies and Research

Prof. Dr. Elvan Yılmaz
Director

I certify that this thesis satisfies the requirements as a thesis for the degree of Master of Science in Electrical and Electronic Engineering.

Prof. Dr. Aykut Hocanın
Chair, Department of
Electrical and Electronic Engineering

We certify that we have read this thesis and that in our opinion it is fully adequate in scope and quality as a thesis for the degree of Master of Science in Electrical and Electronic Engineering.

Prof. Dr. Runyi Yu
Supervisor

Examining Committee

1. Prof. Dr. Runyi Yu
2. Prof. Dr. Hüseyin Özkaramanlı
3. Assoc. Prof. Dr. Hasan Demirel

ABSTRACT

In this work we study the shifted linear interpolation (SLI) method and apply this method in wavelet domain in addition to the spatial domain. The SLI is computationally cheaper than the cubic interpolation and a little more computationally complicated than the standard linear in this way: the computed optimal shift for the SLI is used to change coefficients amplitude and location of the standard linear interpolation. In the spatial domain we achieve a noticeable improvement over the standard linear interpolation in cost of some simple computations. We compare the SLI with other interpolation methods in practical test to ensure its superiority over others. We then evaluate the SLI in wavelet domain, so we carry out our experimental tests in this domain. The SLI method is originated from the principle attempt to minimizing the least square error which is much in the case of the standard linear interpolation.

We Evaluate the SLI with experimental results such as rotation and magnification in spatial and wavelet domain. In rotation experiment, we use the SNR and SSIM to evaluate the standard linear, the SLI, and the cubic methods and this comparison is carried out in spatial domain. A second practical experiment is magnification which is done in spatial as well as wavelet domain and the comparison between the nearest, the standard linear, the SLI and the cubic is hold by visual and objective evaluation.

Keywords: Linear interpolation, Shifted linear interpolation, Super resolution, Spline functions, Discrete wavelet transform.

ÖZ

Bu tez çalışmasında kaydırılmış bir çizgisel enterpolasyon (KÇE) yöntemi üzerinde çalışılmış olup yöntem zaman alanına ek olarak dalgacık alanında da dikkate alınmıştır. Çalışma sonucunda basit hesaplama maliyeti ile standart çizgisel enterpolasyon ile doğru orantılı olarak dikkate alınabilecek bir gelişme sağlanmıştır. Diğer yöntemlere üstünlüğü tespit edilmek üzere, KÇE, diğer enterpolasyon yöntemleri ile deneysel olarak karşılaştırılmıştır. Son olarak KÇE'nin dalgacık alanında değerlendirilmesi kararlaştırılmış olup bu neden ile deneysel testler bu alanda gerçekleştirilmiştir.

KÇE yönteminin kökeni, daha çok standart çizgisel enterpolasyon konusundaki en düşük kare hatasının en düşük düzeye indirgenmesi yönündeki temel girişimlere dayanmaktadır. KÇE hesaplama açısından kübik enterpolasyondan daha ucuz olup hesaplama karmaşıklığı standart çizgisel enterpolasyondan açıklanan şekilde biraz daha fazladır : KÇE için hesaplanan optimum kayma, standart çizgisel enterpolasyonun katsayı değeri ve konumunun değiştirilmesi için kullanılmış olup daha sonra ise standart çizgisel enterpolasyon yöntemi uygulanmıştır.

KÇE yöntemi, zaman ve dalgacık alanlarında rotasyon ve büyütme gibi deneysel sonuçlar ile analiz edilmiştir. Rotasyon deneyinde, standart çizgisel, KÇE ve kübik yöntemlerinin değerlendirilmesi için SNR ve SSIM kullanılmış olup bu karşılaştırma zaman alanında gerçekleştirilmiştir. İkinci deneysel bir test ise büyütme deneyi olup hem zaman hem de dalgacık alanlarında gerçekleştirilmiş olup en yakın, standart

çizgisel, KÇE ve kübik yöntemleri arasındaki karşılaştırma görsel değerlendirme yolu ile geçekleştirilmiştir.

Anahtar Kelimeler: parçalı çizgisel polinomlar, enterpolasyon, hata analizleri, yaklaşma yöntemleri, şerit fonksiyonları, ayrık dalgacık dönüştürme

ACKNOWLEDGMENTS

Thank you, first and foremost, to my research advisor, Prof. Dr. Runyi Yu, who made this project possible and who has always encouraged me and supported my interests. I am honored to have had the chance to study under the guidance of him.

I would like to acknowledge the Eastern Mediterranean University and all faculty members in the Electrical and Electronic department for their unavoidable support to me during my M.S studies. The experience I gained studying at EMU during the past three years was definitely invaluable. I am grateful to have been given many opportunities and have learned much more than I have imagined while studying for my M.S degree.

At last, but definitely not least, thanks to all my family members and my best friend, Vahid, who have helped me throughout my arduous endeavor; their support made it possible to complete my thesis. Their understanding, love is unending and has been present since our beginning, and without them I could not be able to finish it.

Thank you my dear GOD

TABLE OF CONTENTS

ABSTRACT iii

ÖZ iv

ACKNOWLEDGMENTS vi

LIST OF FIGURES ix

LIST OF TABLE xii

LIST OF SYMBOLS/ABBREVIATIONS xiii

1 INTRODUCTION 1

1.1 Introduction 1

1.2 Organization 3

2 INTERPOLATION 5

2.1 Interpolation Methods 5

2.1.1 The Nearest Neighbor Interpolation 7

2.1.2 The Linear Interpolation 8

2.1.3 The Cubic Interpolation 8

2.1.4 The Shifted Linear Interpolation [3] 8

2.2 Approximation by Interpolation 9

2.2.1Measuring Interpolation Error 11

2.2.2 Asymptotic Interpolation Error 13

2.2.3 The Optimal Shift 14

2.3 SNR 14

2.4 PSNR 14

2.5 SSIM 15

3 EXPERIMENTAL RESULTS 18

3.1 Image Interpolation in Spatial Domain 18

3.1.1 Rotation Experiments 20

3.1.2 Zooming Experiments 25

3.2 Image Interpolation in Wavelet Domain 32

3.2.1 Rotation Experiment in Wavelet Domain 33

3.2.2 Zooming Experiment in wavelet domain 37

3.3 Comparison between the Spatial and Wavelet domain 44

CONCLUSION 47

4.1 Conclusion and Future Work 47

REFERENCES 50

LIST OF FIGURES

Figure 3.1: Counter clockwise rotated Lena image by 24° degree 20

Figure 3.2: Rotation experiment algorithm for fifteen times of 24° degree 21

Figure 3.3: Fifteen alternating rotation experiments with 24°of the Lena image, we observe that the SLI image is the sharpest with the highest SNR and SSIM. 22

Figure 3.4: Fifteen alternating rotation experiments with 24°of the Zebra image, we observe that the SLI image is the sharpest one with the highest SNR and SSIM. 23

Figure 3.5: Fifteen alternating rotation experiments with 24°of the Finger-print image, we observe that the SLI image is the sharpest with the highest SNR and SSIM. 23

Figure 3.6: a) Scaled the Zebra image by two: a1) nearest, a2) linear, a3) SLI, and a4) cubic interpolation, the sharpest image belongs to the SLI's image. b) Zoomed images b1, b2, b3 and b4 of a1, a2, a3, and a4, respectively. .. 26

Figure 3.7: a) Scaled the finger-print image by two a1) nearest, a2) linear, a3) SLI, and a4) cubic interpolation, the sharpest image belongs to the SLI's image. b) Zoomed images b1, b2, b3 and b4 of a1, a2, a3, and a4, respectively. .. 27

Figure 3.8: a) Scaled the Lena image by two a1) nearest, a2) linear, a3) SLI, and a4) cubic interpolation, the sharpest image belongs to the SLI's image. b) Zoomed images b1, b2, b3 and b4 of a1, a2, a3, and a4, respectively. .. 28

Figure 3.9: Visual comparison of Finger-print image, a1) original image, a2) linear, a3) SLI, a4) cubic interpolation. 29

Figure 3.10: Visual comparison of Zebra image, a1) original image, a2) linear, a3) SLI, a4) cubic interpolation. 30

Figure 3.11: Visual comparison of Finger-print image, a1) original image, a2) linear, a3) SLI, a4) cubic interpolation. 31

Figure 3.12: Rotational experiment algorithm for fifteen times of 24° degree in wavelet domain. 373

Figure 3.13: Scaled the Lena image by two: a1) nearest, a2) linear, a3) SLI, and a4) cubic interpolation, the sharpest image belongs to the SLI's image. b) Zoomed images b1, b2, b3 and b4 of a1, a2, a3, and a4, respectively. .. 34

Figure 3.14: Scaled the Zebra image by two: a1) nearest, a2) linear, a3) SLI, and a4) cubic interpolation, the sharpest image belongs to the SLI's image. b) Zoomed images b1, b2, b3 and b4 of a1, a2, a3, and a4, respectively. .. 35

Figure 3.15: Scaled the zebra image by two: a1) nearest, a2) linear, a3) SLI, and a4) cubic interpolation, the sharpest image belongs to the SLI's image. b) Zoomed images b1, b2, b3 and b4 of a1, a2, a3, and a4, respectively. .. 35

Figure 3.16: Scaled 2 times the wavelet decomposition of an image in one stage by interpolation methods and subsequent inverse transform respectively...37

Figure 3.17: Scaled the Lena image by two: a1) nearest, a2) linear, a3) SLI, and a4) cubic interpolation, the sharpest image belongs to the SLI's image. b) Zoomed images b1, b2, b3 and b4 of a1, a2, a3, and a4, respectively....38

Figure 3.18: Scaled the Zibra image by two: a1) nearest, a2) linear, a3) SLI, and a4) cubic interpolation, the sharpest image belongs to the SLI's image. b) Zoomed images b1, b2, b3 and b4 of a1, a2, a3, and a4, respectively....39

Figure 3.19: Scaled the Finger-print image by two: a1) nearest, a2) linear, a3) SLI, and a4) cubic interpolation, the sharpest image belongs to the SLI's image. b) Zoomed images b1, b2, b3 and b4 of a1, a2, a3, and a4, respectively....40

Figure 3.20: S Visual comparison of Lena image, a1) original image, a2) linear, a3) SLI, a4) cubic interpolation.. 41

Figure 3.21: S Visual comparison of Zebra image, a1) original image, a2) linear, a3) SLI, a4) cubic interpolation.. 42

Figure 3.22: S Visual comparison of Finger-print image, a1) original image, a2) linear, a3) SLI, a4) cubic interpolation.. 43

Figure 3.23: Visual comparison of Lena image in Spatial and Wavelet domain..... 44

LIST OF TABLE

Table 3.1: Contrast table of the SNR and SSIM with linear, shifted linear, and cubic interpolation. 24

Table 3.2: SNR, PSNR, and SSIM results of linear, shifted linear, and cubic interpolation for rotation experiment. 24

Table 3.3: SNR, PSNR, and SSIM results of linear, shifted linear, and cubic interpolation for zoom experiment.. 32

Table 3.4: SNR, PSNR, and SSIM results of linear, shifted linear, and cubic interpolation for rotation experiment.. 36

Table 3.5: SNR, PSNR, and SSIM results of linear, shifted linear, and cubic interpolation for rotation experiment.. 36

Table 3.6: SNR, PSNR, and SSIM results of linear, shifted linear, and cubic interpolation for zoom experiment.. 44

Table 3.7: Zoom comparisons of spatial and wavelet domain. 45

LIST OF SYMBOLS/ABBREVIATIONS

a_k	Coefficient of Piecewise Polynomial
c_n	Sampling Shifted Linear Interpolation Coefficient
$c(x, y)$	The Contrast Comparison of the Two Dimensional Function
C_{φ}^{int}	The Interpolation Constant of the Asymptotic Interpolation Error
$C_{\varphi}^{\min}$	The Interpolation Constant of the Asymptotic Orthogonal Projection Error
E_{int}	The Interpolation Error
f_n	The Uniform Samples of the Original Continuous Function
$f(x)$	An Original Continuous Function
$f_T(x)$	The Interpolated Function
H_τ	The Casual Pre-Filter of the Shifted Linear Interpolation
$H\left(e^{j\omega}\right)$	The Z Transform of the Filter Coefficient
h_n	The Casual Filter Coefficient
L^2	The Least Square Norm
$l(x, y)$	The Luminance Comparison of the Two Dimensional Function
$P_k(x)$	The Piecewise Polynomial of Degree k
P_T	The Orthogonal Projection
Q_T	The Approximation Function
sinc(x)	The Sinc Function
$s(x, y)$	The Structure Comparison of the Two Dimensional Function

T	The Sampling Step
α	The Power of the Luminance Comparison Function
β	The Power of the Contrast Comparison Function
β^M	B-Splines of Order M
γ	The Power of the Structure Comparison Function
ϵ_f	The Least Square Error
μ_{x}	The Mean of Discrete Function x
τ_{opt}	The Optimal Shift of the Shifted Linear Interpolation
φ_{int}	An Interpolation Function
$\varphi_{sep}(x)$	The Separable Interpolation Basis Function
DWT	Discrete Wavelet Transformation
IDWT	Inverse Discrete Wavelet Transform
SLI	Shifted Linear Interpolation
SNR	Signal to Noise Ratio
SSIM	Structural Similarity Image Quality

Chapter 1

INTRODUCTION

1.1 Introduction

In this thesis, in both spatial and wavelet domain we investigate the shifted linear interpolation (SLI). Our main concern is the applicability of the SLI, first proposed by Blue, Thevenaz, and Unser on May 2004 in [1] , in image super-resolution. Having uniform data samples, the standard linear interpolation interpolates new desired samples by implementing line segments between known samples, whereas the SLI firstly alters the amplitude of known samples and subsequently shifts them, finally, exploits the same line segments as the standard one's to interpolate new samples. The amount of change in amplitude and place of samples for the SLI is chosen in an optimal way that results in a considerable improvement in compare to the standard linear interpolation.

We study the non-adaptive linear interpolation methods that suffer from edge halo, blurring effect and aliasing effect. The reason of these undesired properties is that the non-adaptive methods don't consider the relation between discrete data. In spite of these apparent drawbacks, we are highly inclined to implement the non-adaptive ones because of their explicit algorithms and consequently time-saving algorithms. Performance and computational cost are two major determinants of choosing between interpolation methods, so we need to strike a balance between the needs of the fast algorithm as well as good image with less undesired mentioned effects.

It has been displayed, in [1] and [2] that the quality of standard interpolation methods is outperformed by the projection methods in the least square error sense. Particularly, the standard linear interpolation shows weak performance in compare to the least-squares method in [1] and [2]. We explore SLI which decreases noticeably the least square error and carries out the substantial improvement over the standard version. We will illustrate that this optimal approach results in the reduction of aliasing caused by the standard linear interpolation and consequently we have sharper images.

Interpolation instinctively diminishes the change between the intensities of pixels images by estimating new intensities between old intensities. This decrease of high frequencies in image encourages us to apply the wavelet transformation of image to save these high changes proportionally. In this thesis, we use discrete wavelet transformation to extract high frequencies of images for one level and then in the first level of DWT, we magnify four sub-band images by two time. Subsequently, we apply the inverse of the discrete wavelet transform and evaluate images visually. In this domain, we also observe that the SLI produces shaper images in compare to the standard linear interpolation.

In the sequence, we study the SLI from the interpolation error aspect of view. It is shown in [1] that the interpolation error can be remarkably diminished by using the SLI. This method even approaches the orthogonal projection in the case that the sampling steps get close to zero or, equivalently, of very low-pass functions. We investigate L^2norm of the approximation error developed in [3] for choosing the optimal shift of the SLI. After theoretical superiority of the SLI over the standard one, another way to confirm our claims is to implement experimental results. The experimental analyses contribute to a proper evaluation of diverse linear interpolation

methods. In this thesis, we assess the effectiveness of the interpolation methods by means of visual and computational comparison.

First, the visual comparison is carried out by zooming images through using different linear-interpolation methods as well as the SLI. In the image zooming process, the SLI surpasses the standard interpolation one by making images less smooth than the traditional one. In compare to the third order linear interpolation which is called the bi-cubic, the SLI apparently gets closed to it with the benefit of applying less computation.

Second, we measure the difference between the original image and the interpolated one for the performance comparison. We apply numerical comparison methods such as the signal to noise ratio (SNR), the peak signal to noise ratio (PSNR), and the structural similarity image quality (SSIM) [4]. In our comparisons, the SLI exceeds the traditional linear interpolation and even the cubic interpolation method in SSIM. The geometric rotation transformation is a justified assessment [1] that we use, because we rotate an image by a specified angle until we again get the original one and we implement, at each time of the rotation, the particular interpolation method. These subsequent uses of interpolation functions boost the interpolation error therefor it is more convenient to compare the diverse interpolation methods.

1.2 Organization

Chapter two explains piece-wise polynomial [6], [8] that reconstruct the interpolation functions such as the nearest, linear, and cubic interpolation and also their drawbacks such as blurring and aliasing. We briefly depict the mathematical formula of these interpolation methods and also the shifted linear interpolation. Besides, we shortly

explain that the motivation for the SLI comes from the weak performance of the standard linear interpolation in compare to the projection method in [1], [2].

We study the SLI as a solution to minimize the least square error developed in [4] and [6], and based on this principle, we explain the optimal shift required for the SLI [3]. In this thesis, we use the SNR, PSNR, and SSIM as computational comparisons of interpolation methods. These two are shortly described and their mathematical expression is defined in this chapter.

Next, chapter three provides experimental results that indicate imperfections of standard linear interpolation and superiority of its modified version in spatial and wavelet domain. Furthermore, it will be displayed that the optimally-shifted version somehow outweighs the costly cubic interpolation by implementing computational comparisons, such as the SNR, PSNR, and SSIM for the rotation transformation experiment.

Finally, Chapter four summarize the material presented in this thesis. It also discusses possible future work.

Chapter 2

INTERPOLATION

2.1 Interpolation Methods

Interpolation can be considered as a discrete to continuous converter [7]. The general form of interpolation is:

$$f_T(x) = \sum_{n\in\mathbb{Z}} f_n \varphi_{int}\left(\frac{x}{T} - n\right) \tag{2.1}$$

where f_n, is a set of the uniform samples from the original continuous function f(x) and φ_{int} is an interpolation function. In this section, we explore some of the interpolation functions belong to the piecewise polynomials. In general, a typical interpolator φ_{int} of this category is composed of polynomial pieces [6], [8]:

$$P_k(x) = \sum_{l=0}^{N} a_k[l]x^l, \quad \varepsilon_k \le x < \varepsilon_{k+1} \tag{2.2}$$

which are connected together at break points $\varepsilon_0, \varepsilon_1, \dots, \varepsilon_N$ with guaranteed continuity at the break points, this continuity is reached by making the function right continuous for instance $\varphi(\varepsilon_i) = \varphi(\varepsilon_i^+) = P_i(x)$. In the case of uniform interpolating, the break points are taken as $\varepsilon_{k+1} = \varepsilon_k + 1$, so:

$$\varphi_{int} = \sum_{k=0}^{N-1} P_k(x) \tag{2.3}$$

Then the piecewise polynomial interpolator is defined by its support (number of pieces) N. In order to determine the coefficients of the interpolation polynomial of degree M, we need to set some constraints such as, symmetry around the origin, continuity for the polynomial and some of its derivatives. The majority of $(M+1)N$coefficients a_k are chosen to satisfy these constraints. The independent coefficients are used to improve interpolation approximation [6], [8]. Our interest is to find the most regular piecewise polynomials for a given support and degree, so we implement B-splines [9] with the degree M, the support N = M + 1, and K = M – 1 times continuous derivatives. The B-splines are described in this way [9]:

$$\beta^M = \sum_{i=0}^{M+1} \frac{(-1)^i}{M!} \binom{M+1}{i} \left(x + \frac{M+1}{2} - i\right)_+^M \tag{2.4}$$

where x_+^n is the short form of the power function $\max(0, X^n)$ .Another good property of the B-splines functions is that the higher order B-splines can be reached by continual convolutions:

$$\beta^M = \beta^0 * \beta^{M-1} \tag{2.5}$$

We are highly inclined to implement these interpolation functions because of their explicit algorithms, however, they suffer from these drawbacks:

- Blurring

Blurring is a result of the non-ideality of the interpolation function for the pass-band region in the frequency domain. The interpolator doesn't pass all frequencies similar to the ideal low-pass filter it attenuates some of frequencies. The most attenuation

happens at cut-off frequencies, so the interpolators don't act well in edges and result in blurred edges.

- Aliasing

Aliasing is emerged by improper sampling. This is caused by not omitting the undesired frequencies as a result of overlapping of the periodic spectrums around multiples of 2π . We can diminish this effect by sampling our function at proper points. In interpolation process, we first apply the reconstruction operation (fitting the continuous model to discrete data) and subsequently the re-sampling function. Assuming this model, unwanted frequencies can interfere into the pass-band during the process of re-sampling as a result of nonsufficient suppression of the frequency replicas during the previous step of continuous reconstruction. In sequence, we study the interpolation methods in one dimensional space for the sake of simplicity.

2.1.1 The Nearest Neighbor Interpolation

We investigate the nearest-neighbor method which is a simple rectangular function. Therefore this is the most convenient interpolation method from the computational aspect of view but at the price of causing strong blurring and aliasing effects in the interpolated function.

Nearest interpolation is a simple algorithm in one or more dimensions. The simplest method to reconstruct a function is to take for each position the value of the nearest sampling point. This results in a piecewise constant function. We use the following B-spline basis for this method.

$$\beta^0(x) = \begin{cases} 1, & 0 \leq |x| < 0.5 \\ 0, & 0.5 \leq |x| \end{cases} \tag{2.6}$$

2.1.2 The Linear Interpolation

The linear interpolation which is more computationally complicated than the nearest neighbor interpolation and its function is made by convolution of two simple rectangular functions [10]. The linear interpolation is computationally fast, but this method blurs edges. The interpolation kernel can be achieved by convolving the zero-order B-spline by itself and then the consequent function is:

$$\beta^1(\mathrm{x}) = \begin{cases} 1 - |x|, & 0 \le x < 1 \\ 0, & \text{otherwise} \end{cases} \tag{2.7}$$

2.1.3 The Cubic Interpolation

The cubic interpolation is more computationally expensive than the previous ones and its function is described by convolution of four simple rectangular functions [11]. Since cubic makes functions less blurred, jagged edges are more distinguished. Because cubic B-splines are symmetric, they have just to be specified in the interval (0, 2). Mathematically, the cubic B-spline can be written:

$$\beta^2(\mathrm{x}) = \begin{cases} \frac{x^3}{2} - x^2 + \frac{4}{6}, & (0,1) \\ -\frac{x^3}{6} + x^2 - 2x + \frac{8}{6}, & (1,2) \end{cases} \tag{2.8}$$

2.1.4 The Shifted Linear Interpolation [3]

Estimating $f_T(x)$ is done by utilizing lines between $(n-1)T$ and nT in the standaed linear interpolation [10], for some $\tau \in [0, 1/2]$ we apply lines between $(n-1+\tau)T$ and $(n+\tau)T$ in this following interpolation process [3]:

$$f_T(x) = \sum_{n \in \mathbb{Z}} c_n \Lambda\left(\frac{x}{T} - n - \tau\right) \tag{2.9}$$

with

$$c_n = \sum_{k\geq 0} \frac{(-1)^k}{1-\tau} \left(\frac{\tau}{1-\tau}\right)^k f_{n-k} \tag{2.10}$$

Expression (2.10) relates c_n and f_n via the following casual filter H_τ with the following transform:

$$H_\tau(\mathrm{z}) = \frac{1}{1-\tau+\tau \mathrm{z}^{-1}} = \sum_{k\geq 0} \frac{(-1)^k}{1-\tau} \left(\frac{\tau}{1-\tau}\right)^k \mathrm{z}^{-k} \tag{2.11}$$

with $\tau \in \left[0, 1/2\right]$ for having a stable filter, The Fourier transform of the equivalent interpolation used in (2.9) is gained by replacing the response of the filter in (2.11):

$$\hat{\varphi}_{int}(\omega) = e^{-j\omega\tau} H_\tau(e^{j\omega}) \mathrm{sinc}^2\left(\frac{\omega}{2\pi}\right) \tag{2.12}$$

2.2 Approximation by Interpolation

The typical problem of reconstruction of a continuous function $f(x)$ from a sample values with a uniform sampling step T is considered. Typically, the $Q_T f(x)$ is an estimation of $f(x)$ in the sub space V_T; Q_T relies directly on T. A major concern is to measure the difference among $f(x)$ and $Q_T f(x)$. Besides, it is supposed that this change decreases as the sampling step gets smaller. In other words, when T gets to zero, we expect $Q_T f(x)$ to be equal to input function $f(x)$. We consider the interpolation function as an approximation operator through the following general process:

$$Q_T f(x) = f_T(x) = \sum_{n\in\mathbb{Z}} c_n \varphi\left(\frac{x}{T} - n\right) \tag{2.13}$$

Based on the interpolation condition, the coefficients c_n are chosen in a way that $f_T(x)$ is equal to the original function $f(x)$ at uniform samples f_n. Here $\varphi(x)$ is any function with $\int \varphi(x)dx = 1$. In fact, $\varphi(x)$ is not required to be continuous, interpolating, or symmetric. we can describe the interpolation function as the following filtering relation:

$$f_n = \sum_{n\in\mathbb{Z}} \varphi(k-n)\, c_n \tag{2.14}$$

The coefficients c_n can be obtained by convolving the smples f_n with a filter H, the z-transform of this filter is: . $H(\mathrm{z}) = {\sum_n \mathrm{z}^n}\Big/{\sum_n \varphi(n)} = {\sum_n h_n}\Big/{\sum_n \mathrm{z}^n}$

The interpolation formula (2.13) can be substituded by its traditional version in terms of the samples f_n:

$$f_T(x) = \sum_{n\in\mathbb{Z}} f_n \varphi_{\mathrm{int}}\left(\frac{x}{T} - n\right) \tag{2.15}$$

where

$$\varphi_{\mathrm{int}}(x) = \sum_{n\in\mathbb{Z}} h_n \varphi(x-n) \tag{2.16}$$

We can see that the interpolation function $\varphi_{\mathrm{int}}(x)$ is reached by using the filter coefficients to the basis function φ. The explicite fourier transform of the interpolation function is

$$\hat{\varphi}_{\mathrm{int}}(\omega) = H\left(e^{j\omega}\right)\hat{\varphi}(\omega) \tag{2.17}$$

2.2.1 Measuring Interpolation Error

The error induced by the interpolation process will be evaluated using the L^2 norms, this choice makes it possible to obtain an explicit computation of interpolation error. The difference between function $f(x)$ and the approximated one $f_T(x)$ through a natural L^2 approximation error:

$$\epsilon_f = \|f - f_T\|_{L^2(R)} \tag{2.18}$$

Certainly, we can determine a below bound for this approximation error in this way:

$$\epsilon_{\min}(T) = \|f - P_T f\|_{L^2(R)} \tag{2.19}$$

where $P_T f$ is the orthogonal projection of f.

It would be very convenient to have a quantitative way for choosing the optimal $\varphi$for the interpolation process which minimize the L^2 approximation error $\epsilon_f = \|f - f_T\|_{L^2(R)}$. It is proven in [12] that if $f \in W_2^r$ with $r > \frac{1}{2}$ which means that$f(x)$ has at least $\left\lfloor r - \frac{1}{2} \right\rfloor$ continuous derivatives, then the 1D approximation is given by

$$\epsilon_f = \|f - Qf\|_{L^2} = \left[\int \left|\hat{f}(\omega)\right|^2 E(T\omega) d\omega\right]^{\frac{1}{2}} + e(f,T) \tag{2.20}$$

where the correction term $e(f,T) = o(T^r)$ is bounded as:

$$|e(f,T)| \leq KT^r \left\|f^{(r)}\right\|_{L^2} \tag{2.21}$$

with $K = \frac{2}{\pi^r}\sqrt{\zeta(2r)\|E\|_\infty}$.

Where $\zeta(s) = \sum_{n\geq 1} n^{-s}$ and for all real $s > 1$.

The approximation space for the interpolation process which defined by (2.14) is shift integer invariance. Hence, finding a real shift-invariant version of ϵ_f is appealing where we average an error over all feasible real shifts of the input signal. This averaged measure leads us to approximate the exact quantity of ϵ_f.

Suppose that our aim is reconstructing f_ε described as$f(.-\varepsilon)$, where ε is a real number. The resulting error is T periodic of the shift increment ε, i.e., $\epsilon_{f_{\varepsilon+T}} = \epsilon_{f_\varepsilon}$. Hence, a delay-independent version of the approximation error ϵ_f can be attained over the period interval $[0, T]$. Moreover, this delay-independent version is appealing to the signal processors because the start point of signals is not determined .The following expression, which is proven in [4] and [6] is incredibly simple:

$$\eta(T) = \sqrt{\frac{1}{2\pi}\int \left|\hat{f}(\omega)\right|^2 E(\omega T) d\omega} \qquad (2.22)$$

The term $E(\omega)$ in (2.22) individually depends on $\hat{\varphi}$ and can be conveniently described for the orthogonal and interpolation approximation in this way [1]:

- For the orthogonal projection P_T which is realized to minimize the error approximation in the least square sense, so it minimize $E(\omega)$ by having this equality $\tilde{\varphi} = \varphi_d$ in the orthogonal projection

$$E(\omega) = E_{\min}(\omega) = \frac{\sum_{k\in\mathbb{Z}\setminus\{0\}} |\hat{\varphi}(\omega+2k\pi)|^2}{\sum_{k\in\mathbb{Z}} |\hat{\varphi}(\omega+2k\pi)|^2} \qquad (2.23)$$

- For interpolation

$$E(\omega) = E_{\text{int}}(\omega) = \frac{\left|\sum_{k\in\mathbb{Z}\setminus\{0\}} \hat{\varphi}(\omega+2k\pi)\right|^2 + \sum_{k\in\mathbb{Z}\setminus\{0\}} |\hat{\varphi}(\omega+2k\pi)|^2}{|\sum_{k\in\mathbb{Z}} \hat{\varphi}(\omega+2k\pi)|^2} \quad (2.24)$$

2.2.2 Asymptotic Interpolation Error

The distance between $f(x)$ and $f_T(x)$ goes to zero as the sampling step T tends to zero. It can obviously observed from (2.22) that is the case when $E(0) = 0$, if we consider the interpolation related quantity $E_{\text{int}}(0) = 0$ under proportionally weak conditions on $\varphi(x)$ (see [12]) which are $\hat{\varphi}(2k\pi) = 0$ for all $k \in \mathbb{Z}\setminus\{0\}$ and $\hat{\varphi}(0) = 1$, as are explicit from (2.24). It is shown in [4] that a precise general asymptotic behavior of L^2 approximation is:

$$\|f - Q_T f\|_{L^2(R)} \approx C_\varphi \left\|f^{(L)}\right\|_{L^2(R)} T^L T \to 0 \quad (2.25)$$

where Q_T is an integer shift invariant linear approximation, like interpolation and L is the approximation order of the interpolation function, for example, the approximation order of Λ(x) is 2 because it's Fourier transform is $\widehat{\Lambda}(\omega) = \left(\frac{\sin \omega/2}{\omega/2}\right)^2$ and based on the Strang-Fix condition [13], the approximation order is defined in this way : $\hat{\varphi}^{(l)}(2n\pi) = 0$ for $n \in \mathbb{Z}\setminus\{0\}$ and $l = 0 \ldots L-1$.

The asymptotic constant $C_\varphi = \sqrt{E^{(2L)}(0)/2L!}$ is defined for orthogonal projection and interpolation operator as follows:

1. For the orthogonal projection

$$C_\varphi^{min} = \frac{1}{L!}\sqrt{\sum_{k\neq 0} |\hat{\varphi}^{(L)}(2k\pi)|^2} \quad (2.26)$$

2. For the interpolation function

$$C_{\varphi}^{int} = \sqrt{\frac{1}{L!^2}\left|\sum_{k\neq 0}\hat{\varphi}^{(L)}(2k\pi)\right|^2 + \left(C_{\varphi}^{min}\right)^2} \tag{2.27}$$

2.2.3 The Optimal Shift

It is proven in [3] that the equivalent expression of the asyptotic interpolation constant for the τ-shifted linear interpolation is

$$C_{\tau}^{\mathrm{int}} = \sqrt{\frac{1}{4}\left(\tau^2 - \tau + \frac{1}{6}\right)^2 + \frac{1}{720}} \tag{2.28}$$

C_{τ}^{int} for the following optimal choice is minimized

$$\tau_{\mathrm{opt}} = \frac{1}{2}\left(1 - \frac{\sqrt{3}}{3}\right) \approx 0.21 \tag{2.29}$$

2.3 SNR

SNR is defined as the ratio of signal power to the noise power, often expressed in decibels. We consider Let $x = \{x_i | i = 1,2, \dots, N\}$ as our original signal and $y = \{y_i | i = 1,2, \dots, N\}$ as our interpolated version, so we define the SNR for these two signals of the same size in this way:

$$\mathrm{SNR} = 10\log\frac{\sum_{\mathrm{i}=1}^{\mathrm{N}} \mathrm{x_i^2}}{\sum_{\mathrm{i}=1}^{N}(\mathrm{x_i} - \mathrm{y_i})^2} \tag{2.30}$$

where N is the number of points in the signal.

2.4 PSNR

PSNR is the peak signal-to-noise ratio and often expressed in decibels. We consider Let $x = \{x_i | i = 1,2, \dots, N\}$ as our original signal and $y = \{y_i | i = 1,2, \dots, N\}$ as our

interpolated version, so we define the PSNR for these two signals of the same size in this way:

$$MSE = \frac{1}{N^2}\sum_{\mathrm{i}=1}^{N}(\mathrm{x_i} - \mathrm{y_i})^2 \tag{2.31}$$

$$\mathrm{PSNR} = 10\ \log\frac{MAX_{x_i}^2}{MSE} \tag{2.32}$$

where N is the number of points in the signal.

2.5 SSIM

In this thesis, we apply the structural similarity image quality for [5] comparing interpolation methods. The SSIM is based on the assumption that the human visual system is highly inclined to take part structural information from the image, so a measure of structural similarity can guarantee a good approximation to evaluate image quality.

Let $x = \{x_i | i = 1,2, \dots, N\}$ and $y = \{y_i | i = 1,2, \dots, N\}$ be the original image signals which have been compared with each other to evaluate how much they are similar to each other from human visual system. If we assume that one of the signals is the original one, then the similar measure can be considered as a quantitative measurement of the quality of the second signal. The SSIM is composed of: luminance, contrast and structure. First, the luminance of each signal is compared. We estimate the mean intensity of the assumed discrete signal x :

$$\mu_{\mathrm{x}} = \frac{1}{\mathrm{N}}\sum_{i=1}^{\mathrm{N}}\mathrm{x_i} \tag{2.33}$$

The luminance comparison function is then a function of μ_x and μ_y:

$$l(x,y) = \frac{2\mu_x\mu_y + C_1}{\mu_x^2 + \mu_y^2 + C_1} \tag{2.34}$$

where C_1 is a constant parameter

Second, we remove the mean intensity from the signal. In discrete form, the resulting signal $x - \mu_x$ corresponds to the projection of vector x onto the hyperplane defined by $\sum_{i=1}^{N} x_i = 0$.We apply the standard deviation (the square root of variance) as an estimate of the image contrast. An unbiased estimate of the standard deviation is:

$$\sigma_x = \left(\frac{1}{N-1} \sum_{i=1}^{N} (x_i - \mu_x)^2 \right)^{\frac{1}{2}} \tag{2.35}$$

The contrast comparison $c(x,y)$ is

$$c(x,y) = \frac{2\sigma_x\sigma_y + C_2}{\sigma_x^2 + \sigma_y^2 + C_2} \tag{2.36}$$

where C_2 is a constant parameter

Third, the signal is divided by its own standard deviation, so the two images being compared have unit standard deviation. The structure comparison $s(x,y)$ is conducted on these normalized signals $\frac{(x-\mu_x)}{\sigma_x}$ and $\frac{(y-\mu_y)}{\sigma_y}$ in the following way:

$$s(x,y) = \frac{\sigma_{xy} + C_3}{\sigma_x\sigma_y + C_3} \tag{2.37}$$

where C_3 is a constant parameter. Finally, the three components are combined to yield SSIM:

$$\mathrm{SSIM}(x, y) = ([l(x, y)]^{\alpha}.[c(x, y)]^{\beta}.[s(x, y)]^{\gamma}) \tag{2.38}$$

Where α, β and γ are determined with respect to their importance. In this work, we set $= \beta = \gamma = 1$.

Next, chapter 3 we will depict our experimental results.

Chapter 3

EXPERIMENTAL RESULTS

3.1 Image Interpolation in Spatial Domain

In this chapter, we intend to expand the previous one-dimensional expressions for image processing applications [14] therefore we have to impose some constraints on our interpolation functions [6] .We assume that the interpolation φ_{int} or the non-interpolating φ belongs to two dimensional space R^2. We can diminish the computational cost by assuming that interpolation basis functions are separable. We define their separability in this way:

$$\varphi_{sep}(x) = \varphi(x_1)\varphi(x_2)\,, \quad \forall x_1, x_2 \in \mathrm{R}^2 \tag{3-1}$$

The advantage of this assumption is that we are able to carry out the interpolation process on each dimension separately. For example, images can be analyzed separately, row by row, column by column, and so forth.

We can generalize expression (2.14) for separable basis functions of a two dimensional space:

$$Q_T f(x_1, x_2) = f_T(x_1, x_2) = \sum_{n,l \in \mathbb{Z}} c_{n,l} \varphi\left(\frac{x_1}{T} - n\right) \varphi\left(\frac{x_2}{T} - l\right) \tag{3-2}$$

where $c_{n,l}$ for images can also be computed from uniform samples of image in a separable manner. We write the L^2 approximation error for images in the following way [4] and [6]

$$\epsilon_f{}^2(T) = \|f - f_T\|^2_{L^2(R^2)} = \iint_{-\infty}^{\infty} \big(f(x_1, x_2) - f_T(x_1, x_2)\big)^2 dx_1 dx_2 \tag{3-3}$$

The related formula for (2.23) is [4] and [6]

$$\eta^2(T) = \frac{1}{2\pi} \iint_{-\infty}^{\infty} \left|\hat{f}(\omega_1, \omega_2)\right|^2 \mathrm{E_{int}}(\omega_1 \mathrm{T}, \omega_2 T) d\omega_1 d\omega_2 \tag{3-4}$$

As one dimensional case, $\hat{f}(\omega_1, \omega_2)$ is the fourier transform of $f \in R^2$ and $\mathrm{E_{int}}$ is its interpolation error kernel [3]:

$$E(\omega_1, \omega_2) = E_{int}(\omega_1, \omega_2) = \frac{\left|\sum_{k\in\mathbb{Z}^2\setminus\{0\}} \widehat{\varphi}(\omega_1+2k\pi, \omega_2+2k\pi)\right|^2 + \sum_{k\in\mathbb{Z}^2\setminus\{0\}} |\widehat{\varphi}(\omega_1+2k\pi, \omega_2+2k\pi)|^2}{\left|\sum_{k\in\mathbb{Z}^2} \widehat{\varphi}(\omega_1+2k\pi, \omega_2+2k\pi)\right|^2} \tag{3-5}$$

The asymptotic function (2.26) can be stated in this manner by applying the Taylor analysis [3]:

$$\|f - Q_T f\|^2_{L^2(R)} \approx \Big[\big(C_\varphi^{\min}\big)^2 \left(\|\partial_x^{\mathrm{L}} f\|^2_{\mathrm{L}^2(\mathrm{R})} + \left\|\partial_y^{\mathrm{L}} f\right\|^2_{\mathrm{L}^2(\mathrm{R})}\right) + \Big(\big(C_\varphi^{\mathrm{int}}\big)^2 - \big(C_\varphi^{\min}\big)^2\Big) \left(\|\partial_x^{\mathrm{L}} f\|^2_{\mathrm{L}^2(\mathrm{R})} + \left\|\partial_y^{\mathrm{L}} f\right\|^2_{\mathrm{L}^2(\mathrm{R})} + 2\langle \partial_x^{\mathrm{L}} f, \partial_y^{\mathrm{L}} f\rangle\right)\Big] \mathrm{T^L} \tag{3-6}$$

By substituting$C_\varphi^{\min}$ and $C_\varphi^{\mathrm{int}}$from (2.27) and (2.28) respectively, We again observe that the difference between the interpolation and orthogonal projection constants is again $\sum_{\mathrm{k}\neq 0} \hat{\varphi}^{(L)}(2k\pi)$, so we don't need to evaluate the optimal shift for images (two dimensional signals). In the sequence, we apply the same shift as the one dimensional for images, i. e, $\tau = 0.21$

3.1.1 Rotation Experiments

We rotate an image for example the Lena image by 24° degree and the rotated image is shown in Fig 3.1.

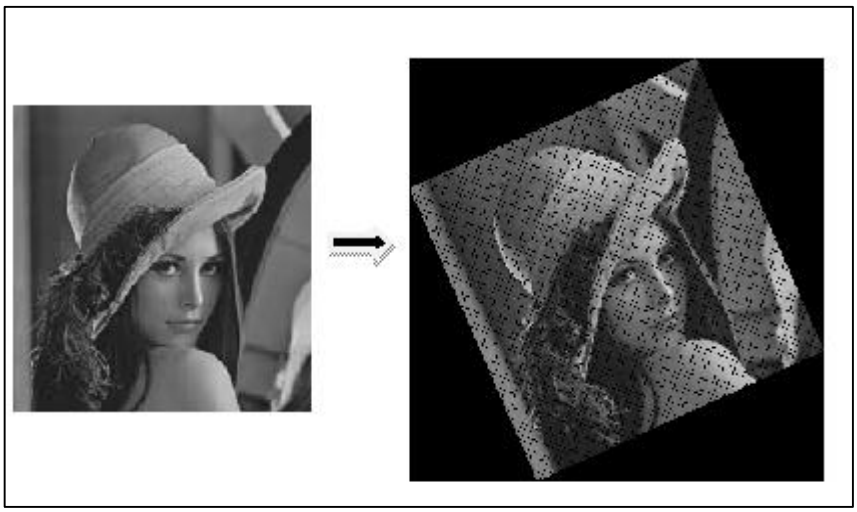

Figure 3.1: Counter clockwise rotated Lena image by 24° degree

As it is shown we lost some pixels through rotating our image, so super resolution is required to enhance the resolution of our image.

In this work, we carry out the super resolution based on the nearest, standard linear, SLI, and cubic interpolation methods. We repeat the rotation and each time we implement the interpolation methods because these subsequent rotations increase the interpolation errors which contribute to better assessment on interpolation functions. We intend to evaluate the interpolation methods from objective point of view, so we hold rotation experiment for fifteen times by 24° degree each time in order to have two same-size images.

We rotate the Lena image and Zebra and Finger-print fifteen times by 24° degree each time. At the last rotation, computing the SNR, PSNR, and SSIM for each image provides computational comparisons for us. We depicts the algorithm of the rotation experiment in the figure 3.2.

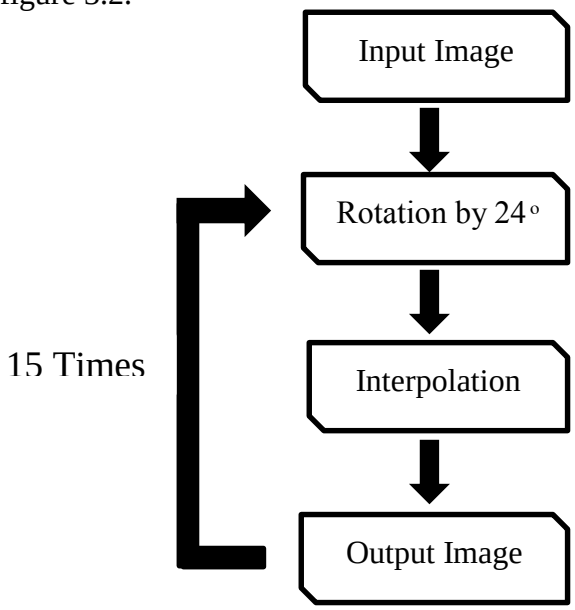

Figure 3.2: Rotation experiment algorithm for fifteen times of 24° degree

We display the fifteenth rotated Lena image in Figure 3.3 and its SNR, PSNR, and SSIM in compare to the original image in Table 3.1. Figure 3.3 clearly shows us the superiority of the SLI method carried out on the Lena image by focusing on edges like her nose, the shadow under her eyes and some parts of her hat that are sharper in SLI's image than others. We also notice her eyelashes which are sharper in SLI's image in compare to other ones images.

The SNR, PSNR, and SSIM values in Table 3.1 also agree with visual comparison in Figures 3.3, 3.4, 3.5. The difference between the SNR, PSNR, and the SSIM values of the Lena image between the SLI and cubic is not too much, but less computational cost of the SLI encourages us to implement the SLI instead of the cubic.

Figure 3.3: Visual comparison of fifteen alternating rotation experiments with $\mathbf{24}^{\circ}$ of the Lena image.

In order to confirm the dominance of SLI over other methods, we decide to apply the SLI on images that possess more edges such as the Zebra and the Finger-print images. As is obviously displayed in Fig.3.4 and Fig.3.5, the SLI beats the standard linear interpolation by producing less noticeably blurred images. Another desiring visual feature of the shifted linear is its sharper images than the cubic interpolated ones. Besides, the SNR, PSNR, and SSIM numbers of images rotated by the SLI method are more than the standard linear and cubic interpolation methods. Fig. 3.4 and 3.5 show the cubic interpolated image in compare to the SLI is a bit more blurred.

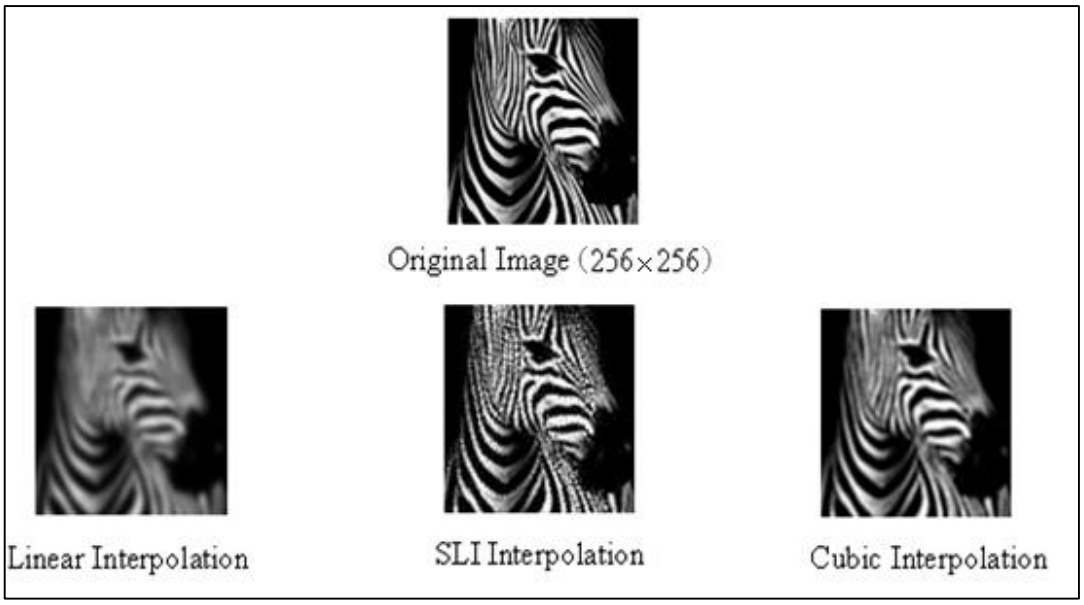

Figure 3.4: Visual comparison of fifteen alternating rotation experiments with 24° of the Zebra image.

Figure 3.5: Visual comparison of fifteen alternating rotation experiments with **24°** of the Finger-print image.

We display the quantitative comparison results of the rotation experiment in the following table. In the Table 3.1, the SNR, SSIM, and PSNR related to the SLI are the highest ones which are in agreement with visual comparisons.

Table 3.1: SNR, PSNR, and SSIM results of linear, shifted linear, and cubic interpolation for rotation experiment.

TESTED IMAGE	SNR(dB)			SSIM			PSNR(dB)		
	LI	SLI	CUBIC	LI	SLI	CUBIC	LI	SLI	CUBIC
LENA	19.73	**25.79**	25.14	0.8	**0.95**	0.93	27.27	**33.22**	32.59
ZEBRA	3.17	**8.74**	7.09	0.43	**0.8**	0.72	11.95	**14.75**	14.70
FINGER-PRINT	12.32	**21.49**	21.33	0.58	**0.95**	0.94	19.00	**28.17**	28.16

We also depict the SNR, PSNR, and SSIM results of the same rotation experiment for thirteen times by 12° degree each time to have better judgment.

Table 3.2: SNR, PSNR, and SSIM results of linear, shifted linear, and cubic interpolation for rotation experiment.

TESTED IMAGE	SNR(dB)			SSIM			PSNR(dB)		
	LI	SLI	CUBIC	LI	SLI	CUBIC	LI	SLI	CUBIC
LENA	17.80	**23.60**	23.19	0.69	**0.92**	0.89	25.70	**32.01**	31.09
ZEBRA	4.7	**8.98**	7.37	0.42	**0.8**	0.71	12.64	**16.75**	15.32
FINGER-PRINT	11.55	**20.37**	20.27	0.30	**0.93**	0.92	15.94	**24.17**	24.65

In this experiment, SLI also outperforms the other methods by its higher quantities.

3.1.2 Zooming Experiments

In this thesis, we are inclined to evaluate the interpolation methods by converting images from low-resolution to high-resolution ones. We carry out the magnification test on the Zebra image Fig.3.6a, the Finger-print image Fig.3.7a, and the Lena image Fig.3.8a. In Fig.3.6, the highest contrast between black and white lines of the Zebra image belongs to the SLI magnified image. In Fig.3.7, we observe that the SLI makes the finger-print image looks brighter than the standard and cubic interpolation's ones and even than the original one. In Fig.3.8, looking at the shadow on Lena's shoulder, noise, and forehead in big images leads us to the sharpest and brightest image which belongs to the SLI. We also display some zoomed parts of all magnified images for having better comparison.

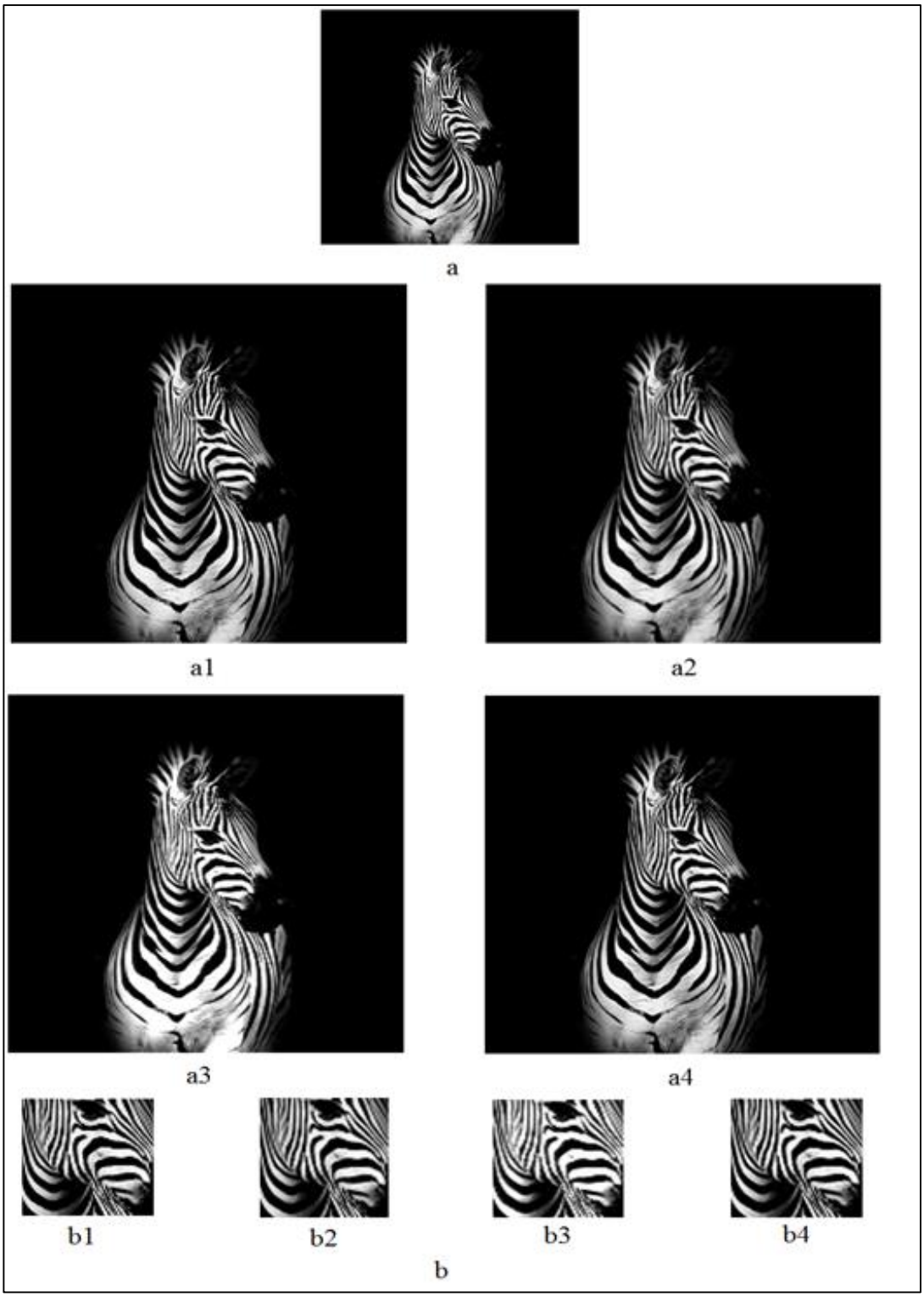

Figure 3.6: a) Scaled the Zebra image by two: a1) nearest, a2) linear, a3) SLI, and a4) cubic interpolation, the sharpest image belongs to the SLI's image. b) Zoomed images b1, b2, b3 and b4 of a1, a2, a3, and a4, respectively.

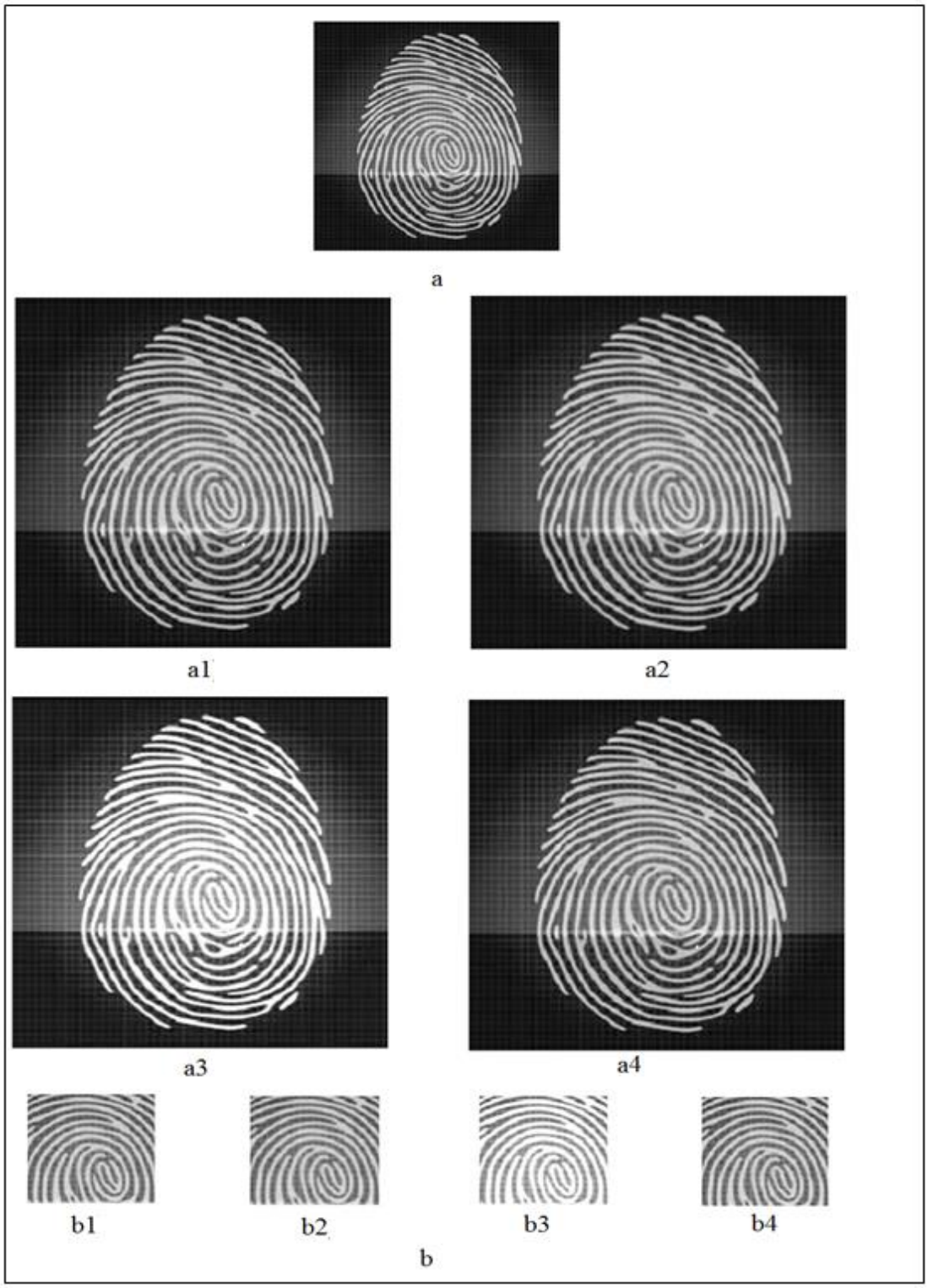

Figure 3.7: a) Scaled the finger-print image by two a1) nearest, a2) linear, a3) SLI, and a4) cubic interpolation, the sharpest image belongs to the SLI's image. b) Zoomed images b1, b2, b3 and b4 of a1, a2, a3, and a4, respectively.

Figure 3.8: a) Scaled the Lena image by two a1) nearest, a2) linear, a3) SLI, and a4) cubic interpolation, the sharpest image belongs to the SLI's image. b) Zoomed images b1, b2, b3 and b4 of a1, a2, a3, and a4, respectively.

All SLI zoomed images are brighter than the original image, this visual feature can be considered as distortion. In order to have objective comparisons, namely, SNR, SSIM, and PSNR for this experiment, we down-sample our test images without using interpolation and then return them back to their original sizes by the linear, SLI, and cubic interpolation methods. Zoomed parts of resulted images together with the related zoomed part of the original image are shown in the Figure 3.9, 3.10, and 3.11.

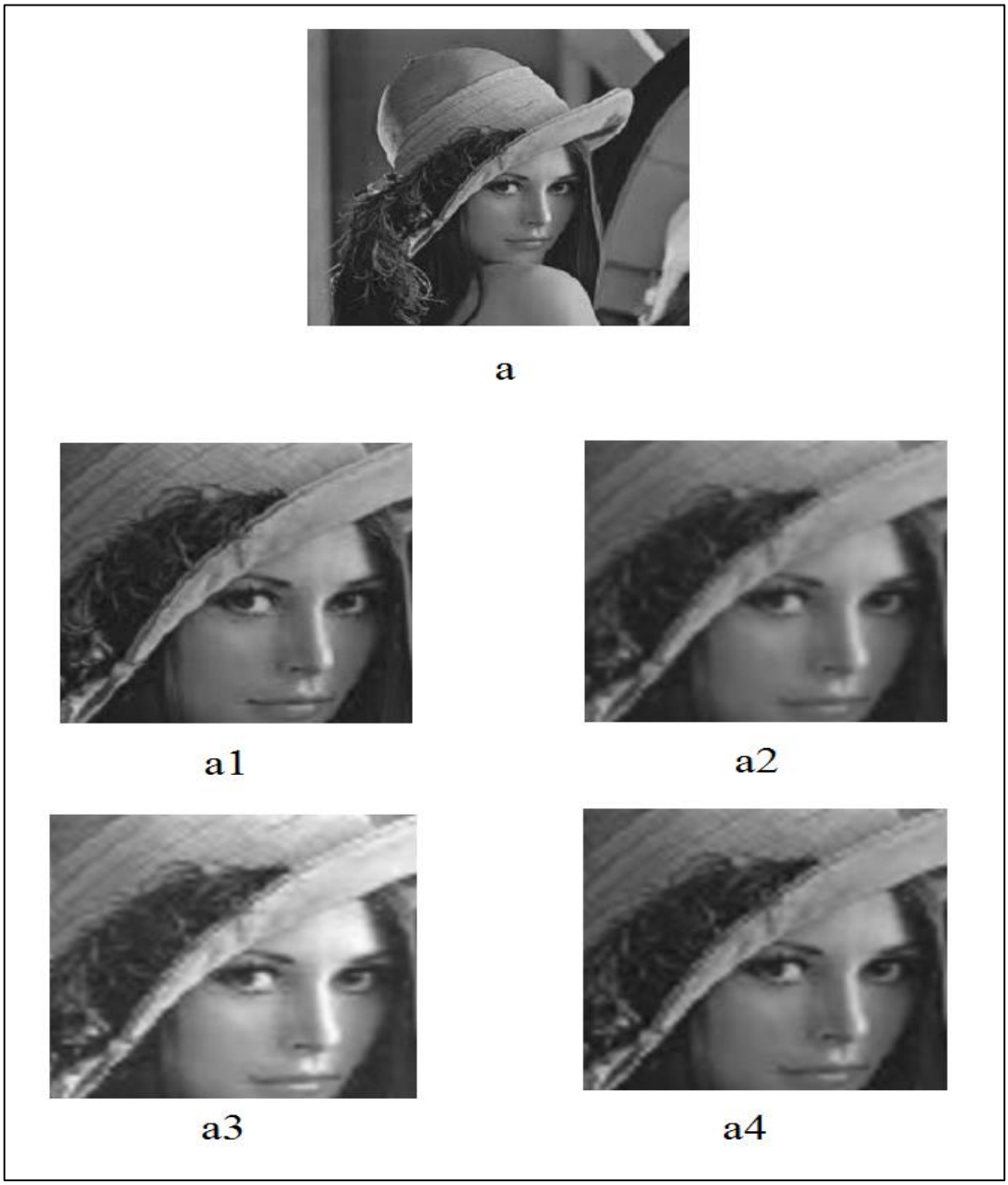

Figure 3.9: Visual comparison of Lena image, a1) original image, a2) linear, a3) SLI, a4) cubic interpolation.

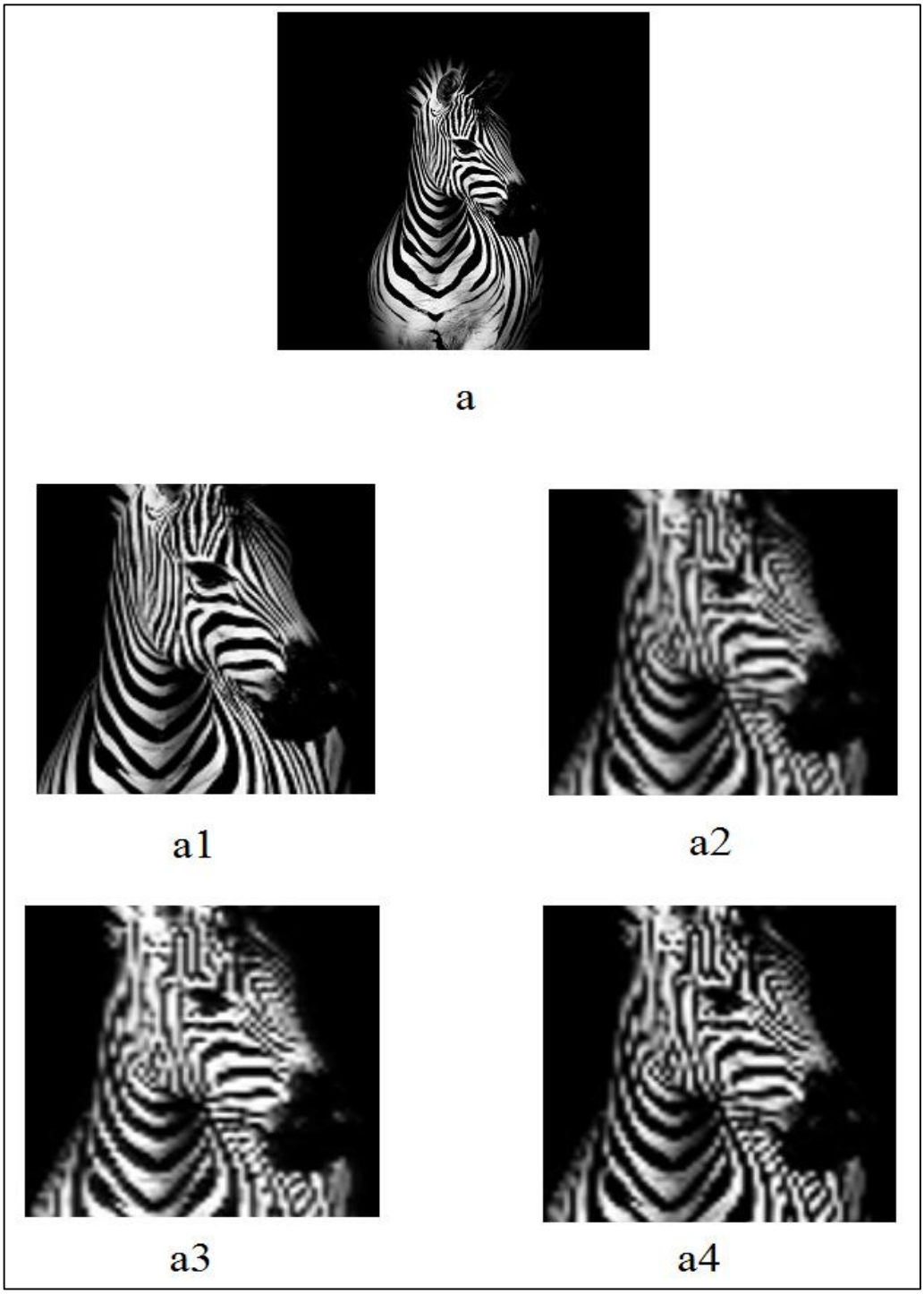

Figure 3.10: Visual comparison of Zebra image, a1) original image, a2) linear, a3) SLI, a4) cubic interpolation.

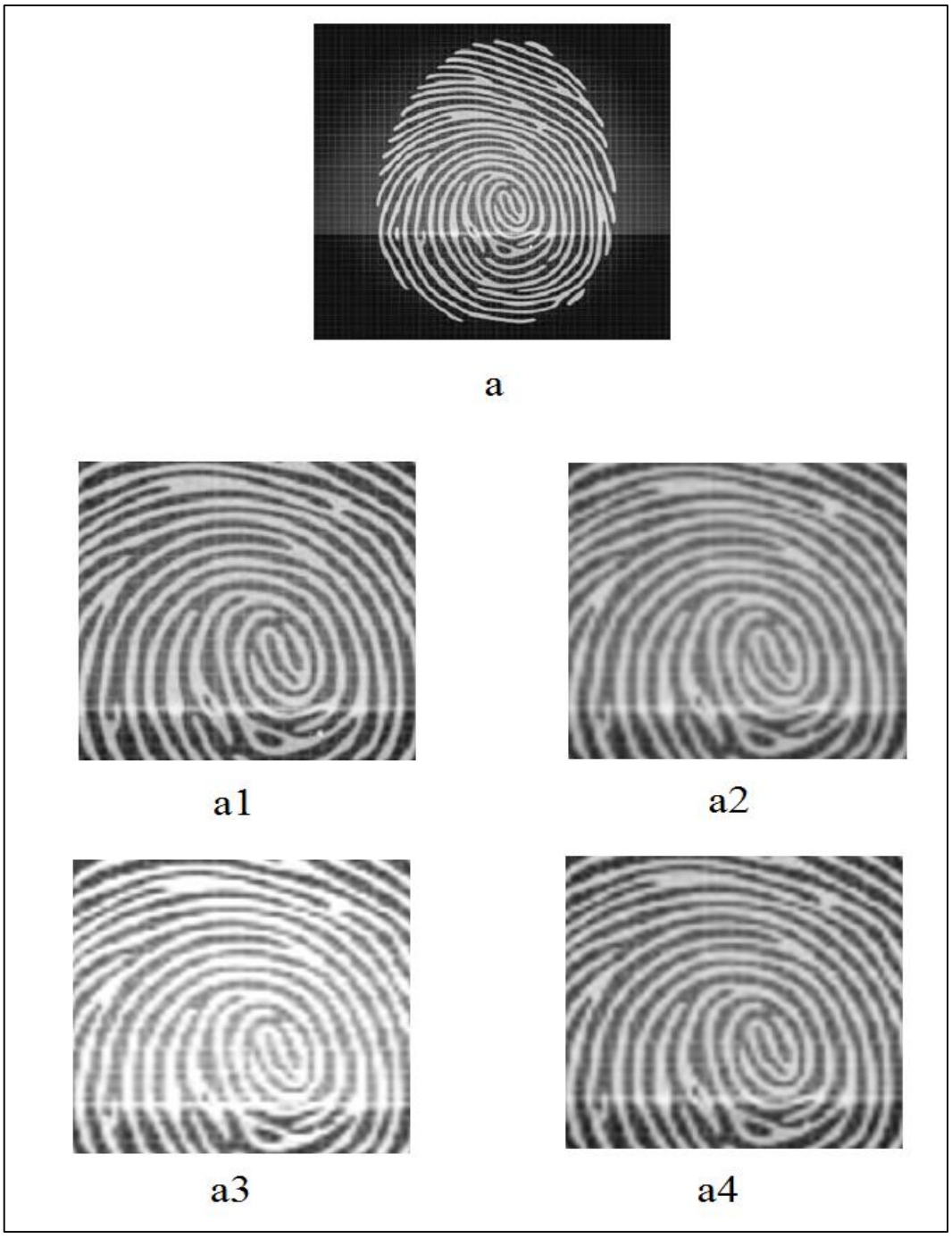

Figure 3.11: Visual comparison of Finger-print image, a1) original image, a2) linear, a3) SLI, a4) cubic interpolation.

We display the computational comparison results of the zoom experiment in the following table. The Table 3.3 states that the SLI method possesses poorer performance in compare to the other methods due to the lowest SLI's quantities of SNR, SSIM, and PSNR. The objective comparison results agree with visual

comparisons, because the SLI significantly makes zoomed images brighter than the original image.

Table 3.3: SNR, PSNR, and SSIM results of linear, shifted linear, and cubic interpolation for zoom experiment.

TESTED IMAGE	SNR(dB)			SSIM			PSNR(dB)		
	LI	SLI	CUBIC	LI	SLI	CUBIC	LI	SLI	CUBIC
LENA	19.91	7.62	19.79	0.82	0.5	0.83	27.81	15.52	27.64
ZEBRA	6.03	2.71	5.78	0.66	0.41	0.68	13.97	10.65	13.72
FINGER-PRINT	15.83	7.04	16.12	0.80	0.38	0.84	20.21	11.42	20.50

3.2 Image Interpolation in Wavelet Domain

Interpolation instinctively diminishes the change between the intensities of pixels image by estimating new intensities between old intensities. This decrease of high frequencies of image encourages us to apply the wavelet-based interpolation. Image resolution enhancement in the wavelet domain is an appealing method to image processors, because we get noticeable improvement in compare to the direct interpolation in spatial domain [15]. Due to the advantages of the wavelet-based interpolation a lot of new algorithms have been proposed such as [16], [17].

In this thesis, we exploit one of the wavelet transformations called the discrete wavelet transformation (DWT) [18] to extract high frequencies of images for one level and then in the first level of DWT [19], we carry out the zoom and rotation experiments over four sub-band images by using interpolation methods. Subsequently, we apply

the inverse of the discrete wavelet transform and evaluate images subjectively and objectively.

3.2.1 Rotation Experiment in Wavelet Domain

In this experiment, we use Daubechies 10 (db10) [20], [19] as a discrete wavelet transform for one level and then we rotate each resulted sub-band images; namely, low-low (LL), low-high (LH), high-low (HL), and high-high (HH), fifteen times by 24° degree to have the same size sub-band images like spatial domain rotation experiment. Finally, we apply IDWT [19] and compare the output image with the original image with SSIM, SNR, PSNR. We depicts the algorithm of this experiment in the figure 3. 12.

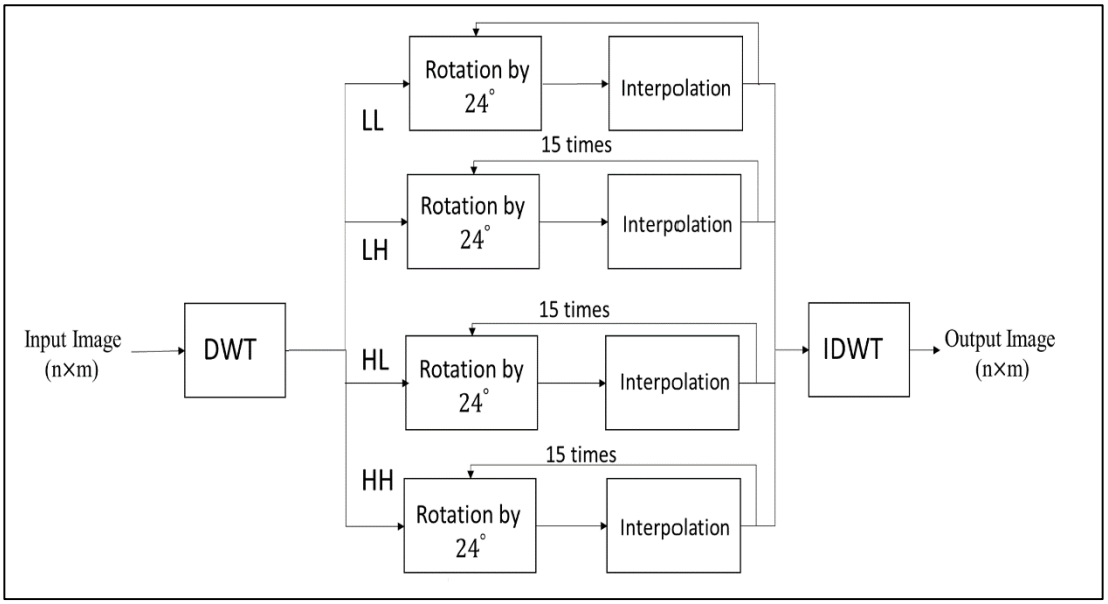

Figure 3.12: Rotation experiment algorithm for fifteen times of 24° degree in wavelet domain

We display the fifteen-time rotated Lena image in wavelet domain in Fig 3.13 and its SNR, SSIM, and PSNR in compare to the original image for the linear, SLI, and cubic interpolation in Table 3.4. Although, visual comparison of resulted images states that the SLI image is sharper than the linear and cubic images, the SLI image suffers from

discontinuities hardly, for example in Lena's eyebrow. From the SNR, SSIM, and PSNR of different interpolation methods in Table 3.4, we conclude that the SLI outperforms the linear interpolation, but it can't reach the SNR, SSIM, and PSNR values of the cubic interpolation for the Lena image.

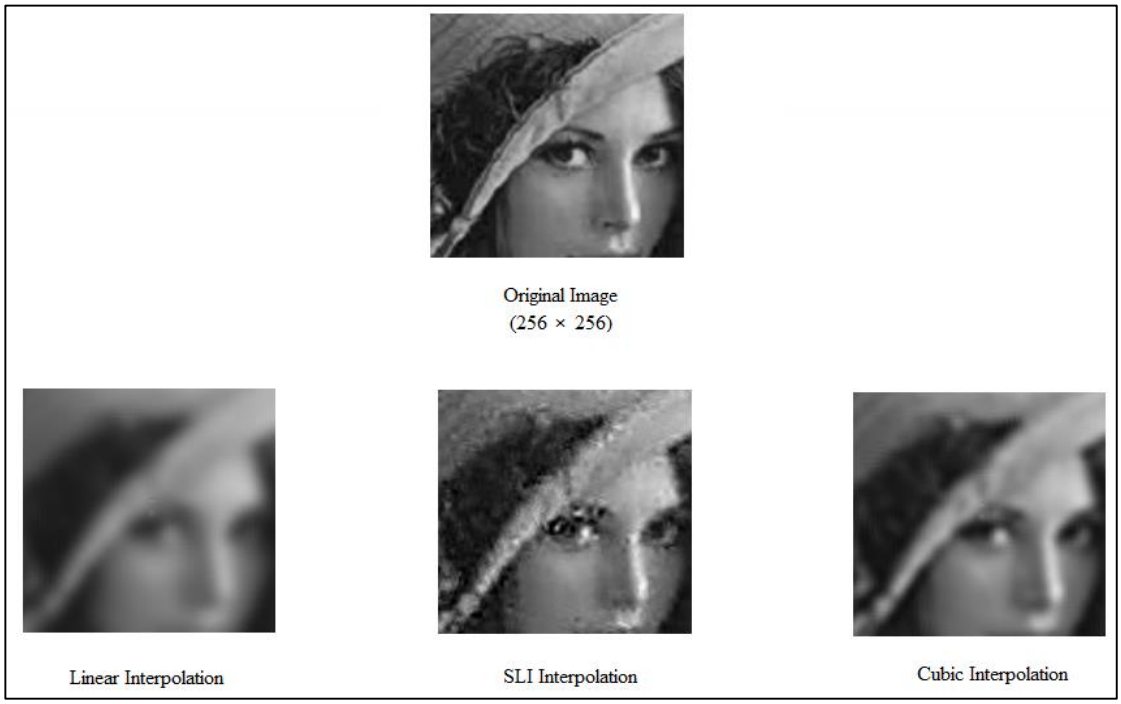

Figure 3.13: Fifteen alternating rotation experiments with 24° of the Lena image in wavelet domain.

In order to better assessment, we decide to do the above experiment on the Zebra and Finger-print images. It is obviously shown in Fig 3.14 and Fig 3.15 that the SLI is again better than the linear interpolation by producing less blurred images in compare to images of the standard linear interpolation. The SLI is even sharper than the Cubic's image. Conversely, for the Zebra image the SNR doesn't agree with our visual comparison and states that the cubic interpolation is the best. For the Finger-print image, visual comparison again admits being more sharpness of the SLI's image than of the other two methods' ones. For this image, the SNR and SSIM agrees with our visual comparison.

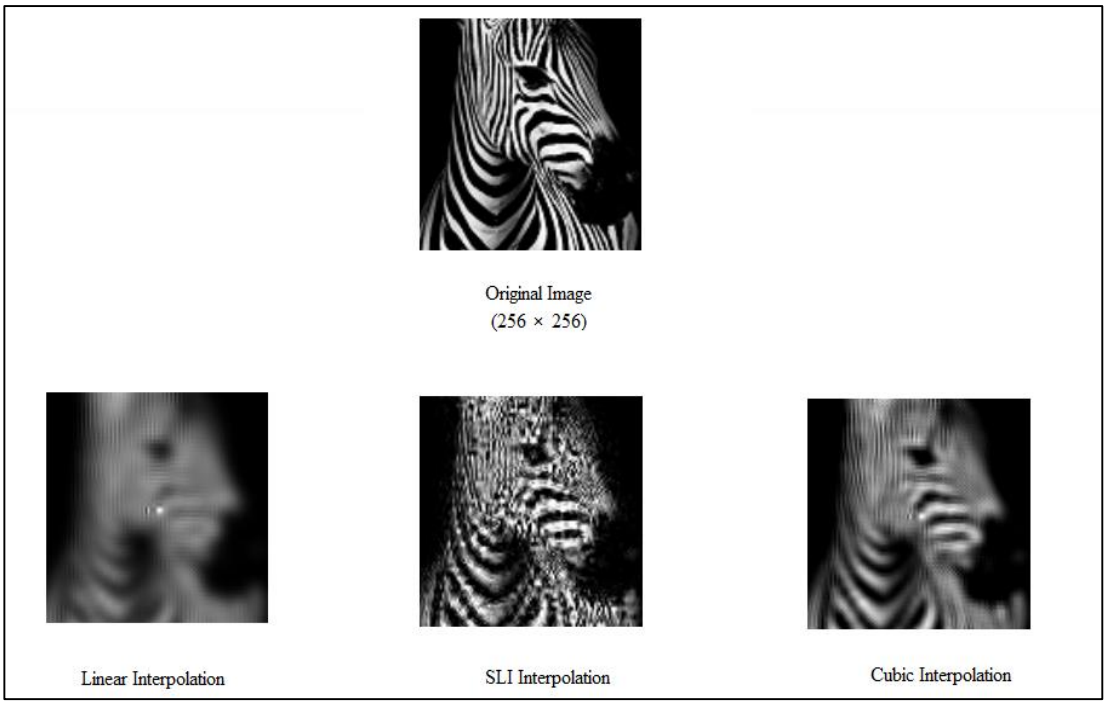

Figure 3.14: Fifteen alternating rotation experiments with 24° of the Zebra image in wavelet domain.

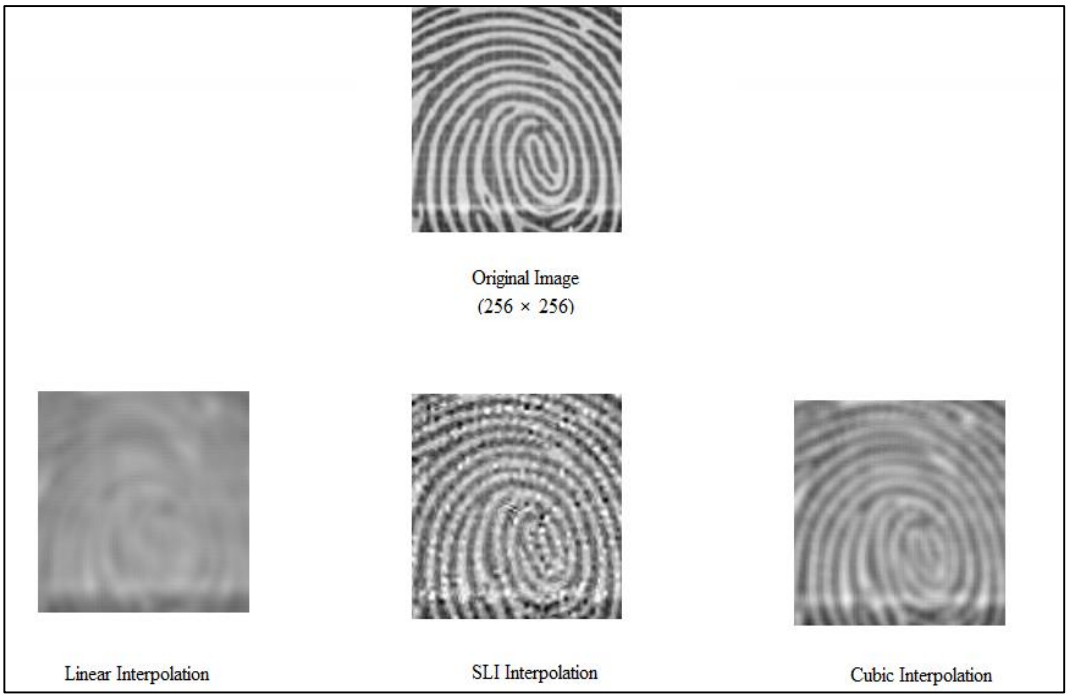

Figure 3.15: Fifteen alternating rotation experiments with 24° of the Finger-Print image in wavelet domain.

We display the computational comparison results of the rotation experiment in wavelet domain in the following table. In Table 3.4, the SNR, SSIM, and PSNR values of the SLI are more than values of the standard linear for all images.

Table 3.4: SNR, PSNR, and SSIM results of linear, shifted linear, and cubic interpolation for rotation experiment.

TESTED IMAGE	SNR(dB)			SSIM			PSNR(dB)		
	LI	SLI	CUBIC	LI	SLI	CUBIC	LI	SLI	CUBIC
LENA	15.14	17.69	18.76	0.45	0.69	0.79	21.82	23.67	25.11
ZEBRA	3.97	4.27	5.57	0.45	0.56	0.58	11.50	11.95	12.30
FINGER-PRINT	11.17	15.12	13.83	0.49	0.82	0.79	18.17	22.12	21.01

We also depict the SNR, PSNR, and SSIM results of the same rotation experiment for thirteen times by 12° degree each time to have better judgment in Table 3.5.

Table 3.5: SNR, PSNR, and SSIM results of linear, shifted linear, and cubic interpolation for rotation experiment.

TESTED IMAGE	SNR(dB)			SSIM			PSNR(dB)		
	LI	SLI	CUBIC	LI	SLI	CUBIC	LI	SLI	CUBIC
LENA	12.88	**15.30**	16.22	0.38	**0.53**	0.68	19.43	**22.01**	23.88
ZEBRA	3.8	**3.9**	4.38	0.41	**0.49**	0.50	12.3	**12.58**	13.4
FINGER-PRINT	10.87	**14.80**	13.67	0.38	**0.78**	0.75	17.78	**20.27**	20.10

3.2.2 Zooming Experiment in Wavelet Domain

In our following experimental results, we use Daubechies 10 (db10) [20], [19] as a discrete wavelet function for one level and we put a factor of magnification equal to two.

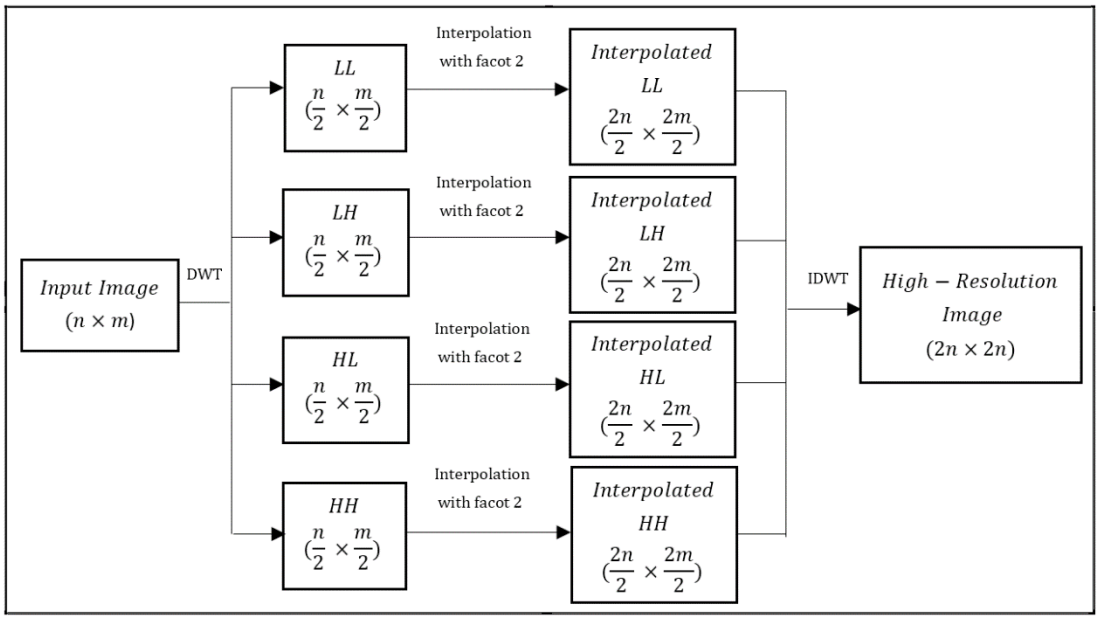

Figure 3.16: Scaled 2 times the wavelet decomposition of an image in one stage by interpolation methods and subsequent inverse transform. [19]

With visual comparison, we conclude that the SLI method performs better than the nearest, linear, even cubic in wavelet domain and produces the sharpest images of them. For example, we can recognize the superiority of the SLI's images by looking at Lena's eyes shadow and lashes which is sharper in SLI's one in Fig.3.17) a3. For the Zebra image, we compare different interpolation's images by evaluating the contrast between black and with lines in Fig.3.18 (a1, a2, a3, and a4). Finally, the Finger-print image also shows that the shifted linear interpolation method produces the sharpest image in compare to others in Fig.3.19 (a3). In order to better evaluation between interpolation methods, we also show zoomed parts of all magnified images in figures Fig.3.17, Fig.3.18, and Fig.3.19.

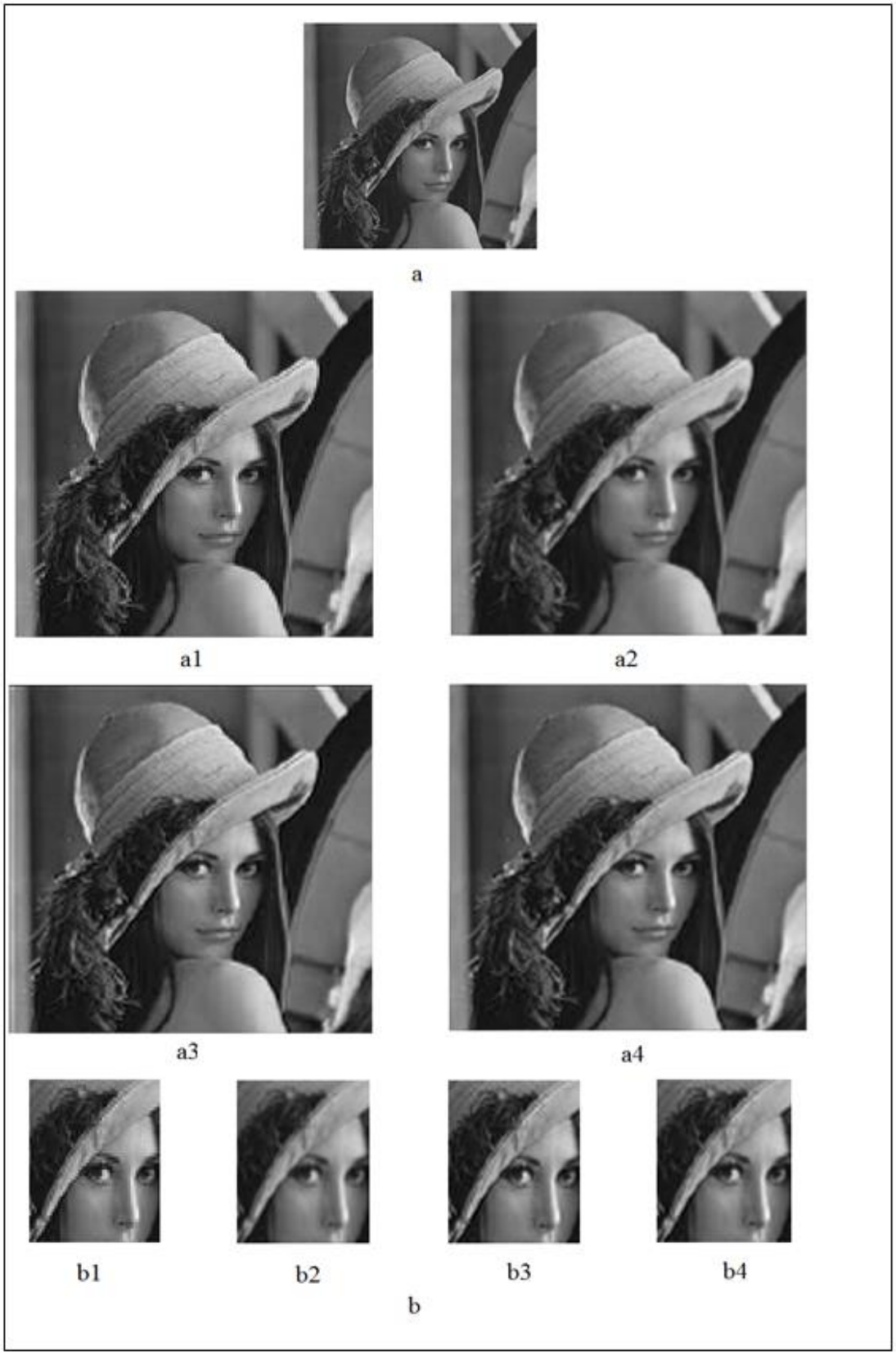

Figure 3.17: Scaled the Lena image by two: a1) nearest, a2) linear, a3) SLI, and a4) cubic interpolation, the sharpest image belongs to the SLI's image. b) Zoomed images b1, b2, b3 and b4 of a1, a2, a3, and a4, respectively.

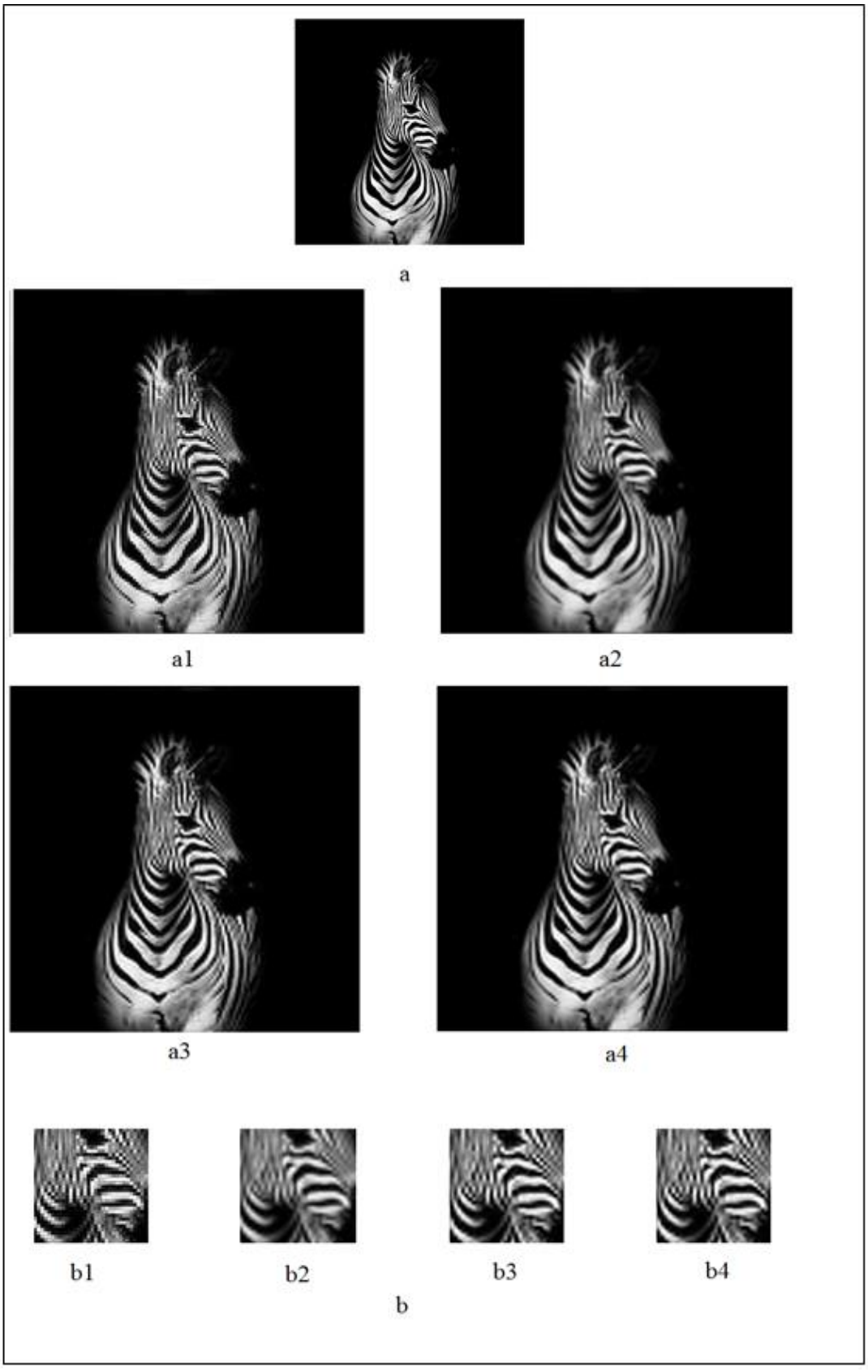

Figure 3.18: Scaled the Zebra image by two: a1) nearest, a2) linear, a3) SLI, and a4) cubic interpolation, the sharpest image belongs to the SLI's image. b) Zoomed images b1, b2, b3 and b4 of a1, a2, a3, and a4, respectively.

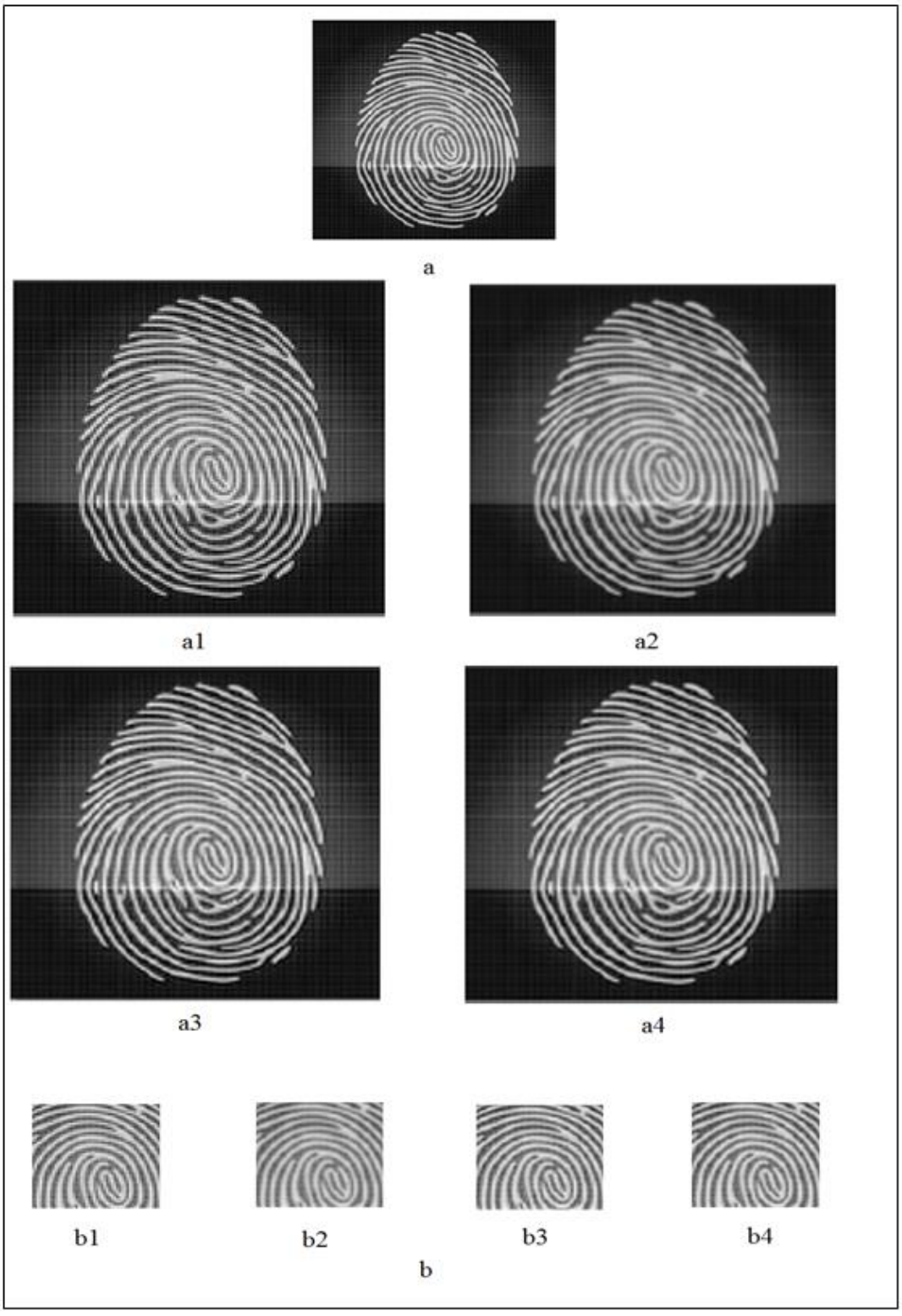

Figure 3.19: Scaled the zebra image by two: a1) nearest, a2) linear, a3) SLI, and a4) cubic interpolation, the sharpest image belongs to the SLI's image. b) Zoomed images b1, b2, b3 and b4 of a1, a2, a3, and a4, respectively.

In order to have objective comparisons, namely, SNR, SSIM, and PSNR for this experiment, we down-sample our test images without using interpolation and then return them back to their original sizes by the linear, SLI, and cubic interpolation methods in wavelet domain. Zoomed parts of resulted images together with the related zoomed part of the original image are shown in the Figure 3.20, 3.21, and 3.22.

Figure 3.20: Visual comparison of Lena image, a1) original image, a2) linear, a3) SLI, a4) cubic interpolation.

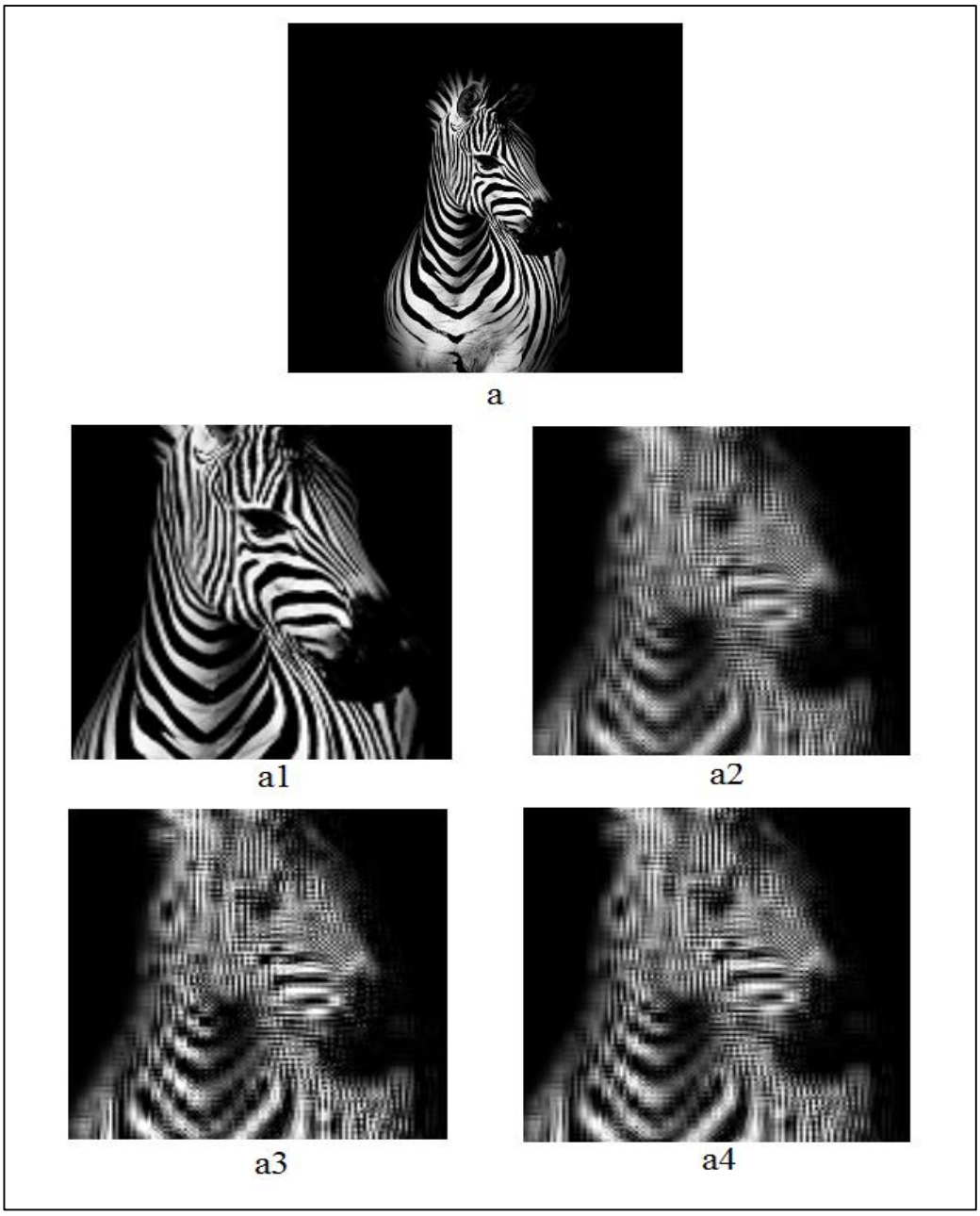

Figure 3.21: Visual comparison of Zebra image, a1) original image, a2) linear, a3) SLI, a4) cubic interpolation.

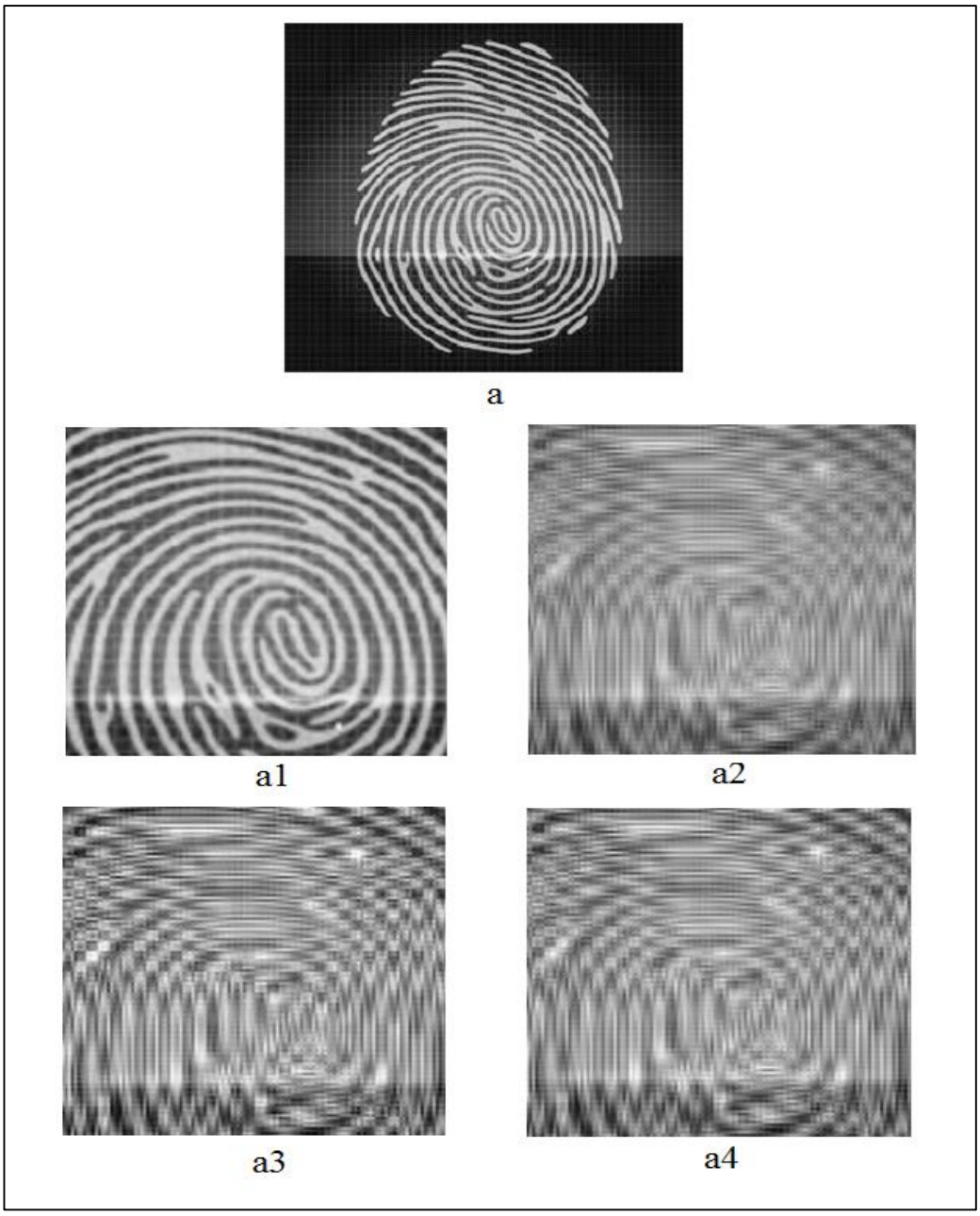

Figure 3.22: Visual comparison of Finger-print image, a1) original image, a2) linear, a3) SLI, a4) cubic interpolation.

We display the computational comparison results of the zoom experiment of the wavelet domain in the Table 3.6. The Table 3.6 shows that the SNR and SSIM of the SLI method possesses higher values in compare to the other methods for the Lena and Zebra image but not for the Finger-print image.

Table 3.6: SNR, PSNR, and SSIM results of linear, shifted linear, and cubic interpolation for zoom experiment.

TESTED IMAGE	SNR(dB)			SSIM			PSNR(dB)		
	LI	SLI	CUBIC	LI	SLI	CUBIC	LI	SLI	CUBIC
LENA	15.24	17.07	14.79	0.65	0.66	0.63	23.32	25.15	22.88
ZEBRA	4.47	4.11	3.89	0.71	0.73	0.71	15.63	15.27	15.66
FINGER-PRINT	8.32	7.60	7.83	0.32	0.35	0.33	16.05	15.33	15.56

3.3 Comparison between the Spatial and Wavelet Domain

We magnify test images by factor two in spatial and wavelet domain and in Fig 3.20, you can compare spatial and wavelet resulted images visually. We observe that the advantage of zoom experiment in wavelet domain is that the zoomed images are not brighter than the original image like spatial domain.

Figure 3.20: Visual comparison of Lena image in Spatial and Wavelet domain

We depicts objective results of zoom experiments in the spatial and wavelet domain in Table 3.7. This table confirms the superiority of the SLI in wavelet domain.

Table 3.7: Zoom comparisons of spatial and wavelet domain

TESTED IMAGE	Spatial Domain									Wavelet Domain								
	SNR(dB)			SSIM			PSNR(dB)			SNR(dB)			SSIM			PSNR(dB)		
	LI	SLI	CUBIC	LI	SLI	CUBIC	LI	SLI	CUBIC	LI	SLI	CUBIC	LI	SLI	CUBIC	LI	SLI	CUBIC
LENA	19.91	7.62	19.79	0.82	0.5	0.83	27.81	15.52	27.64	15.24	17.07	14.79	0.65	0.66	0.63	23.32	25.15	22.88
ZEBRA	6.03	2.71	5.78	0.66	0.41	0.68	13.97	10.65	13.72	4.47	4.11	3.89	0.71	0.73	0.71	15.63	15.27	15.66
FINGER -PRINT	15.83	7.04	16.12	0.80	0.38	0.84	20.21	11.42	20.50	8.32	7.60	7.83	0.32	0.35	0.33	16.05	15.33	15.56

The Table 3.1 in spatial domain and Table 3.4 in wavelet domain recommend using interpolation methods for rotation experiment in spatial domain. The lower quantities of SNR, PSNR, and SSIM regarded to the wavelet domain can be increased by computing new optimal shift for the wavelet domain.

Chapter 4

CONCLUSION

4.1 Conclusion and Future Work

This work is concerned with using the Shifted Linear Interpolation for the super resolution purpose. We explore that the SLI is explicitly originated from altering the standard linear interpolation's samples amplitude and their position with regard to the determined shift. The SLI is motivated with the weak performance of the standard linear interpolation in compare to the projection method in [1], [2]. In this thesis, we carry out interpolation based super resolution via the SLI.

We study the SLI as a solution to minimize the least square error and based on this principle, we explain the optimal shift required for the SLI [3]. Our interest in the SLI originates from its less least square error than of the standard linear interpolation and less computational cost than the cubic interpolation method.

The subjective and objective comparison have applied for comparing the SLI method with other interpolation techniques. We have carried out the magnification experiment for the subjective evaluation and this experiment due to a great demand of big images is appealing. We have zoomed tested images by two time with SLI and compare it visually with other magnified images using nearest, bi-linear, and bi-cubic. We have observed that the SLI zoomed images were brighter than the original image which states that the SLI damages images in compare to the original test image. Besides, for

using quantitative comparisons, we first down-sampled the original image and then converted it to the original size. In this experiment, the SLI performed poorer other interpolation methods.

We rotate our image fifteen times by 24° and 30° degrees and at each time of rotation we apply the SLI. We have done this experiment for other interpolation methods and have used SSIM, SNR, and PSNR for computational comparison. The SSIM, SNR, and PSNR of the SLI have outperformed all of the others. In spatial domain, the SLI has defeated the nearest, bilinear, and bi-cubic interpolation methods.

In this thesis, we have applied the SLI for the super resolution application in wavelet domain. First, discrete wavelet transform [19]changes our image into four different frequency components and then we use interpolation methods to rescale images. Next, we apply the inverse discrete wavelet transform [19]and then we have bigger images related to the scale number. Finally, we compared images visually and recognize that the SLI's images are the sharpest similar to the spatial domain.

We have observed that images interpolated by the SLI in wavelet domain are sharper and not brighter than the original image like spatial domain. This improvement can be referred to the characteristics of discrete wavelet transform which decompose an image into its different frequency components that each of components displays some details of image. The objective comparisons' numbers of zoom experiment in wavelet domain were higher than ones in the spatial domain. We also have carried out the rotation experiment in wavelet domain and haven't got good results. These results can be improved by computing new optimal shift for this domain due to defining our images from spatial domain to wavelet domain.

In this work, practical results prefer using SLI in spatial domain in compare to using it in wavelet domain for rotation experiment and in wavelet domain in compare to using it in spatial domain for zooming experiment.

As a future work we can compute the optimal shift for cubic interpolation method and apply the shifted cubic interpolation in spatial and wavelet domain.

REFERENCES

[1] A. Aldroubi, M. Eden, and M. Unser, "Enlargment or Reduction of Digital Images with Minimum Loss of Information," *IEEE Transaction on Image Processing*, vol. 4, March 1995.

[2] T. Blu, M. Unser, and A. Muñoz, "Least-Square Image Resizing Using Finite Deference," *IEEE Transaction on Image Processing*, vol. 10, September 2001.

[3] Blu, P. Thevenaz, and M. Unser, "Linear Interpolation Revitalized," *IEEE Transaction on Image Processing*, vol. 13, no.5, May 2004.

[4] T. Blue and M. Unser, "Quantitative Fourier Analysis of Approximation Techniques: Part 1 Interpolators and Projectors," *IEEE Transaction on Signal Processing*, vol. 47, no. 10, October 1999.

[5] A.C. Bovik, H.R. Sheikh, E.P. Simoncelli, and Z. Wang, "Image Quality Assessment: From Error Measurment to Structral Similarity," *IEEE Transaction on Image Processing*, vol. 13, January 2004.

[6] T. Blu, M. Unser, P. Thévenaz, "Interpolation Revisited," *IEEE Transaction on Med. Imag*, vol. 19,July 2000.

[7] G.M. Phillips, *Interpolation and Approximation by Polynomials*, 2nd ed., Ed.: Springer, 2003.

[8] P. Thévenaz, M. Unser, and T. Blu, "“MOMS: Maximal-Order Interpolation of Minimal Support," *IEEE Transaction on Image Processing*, vol. 10, July 2001.

[9] M. Unser, "Splines: A Perfect Fit for Signal and Image Processing," *IEEE Signal Process. Mag.*, vol. 16, November 1999.

[10] E. H. W. Meijering, "A Chronology of Interpolation: From Ancient Astronomy to Modern Signal and Image Processing," *Proceeding of the IEEE*, vol. 90, march 2002.

[11] R. G. Keys, "Cubic Convolution Interpolation for Digital Image Processing," *IEEE Transaction on Image Processing*, vol. 29, december 1981.

[12] M. Unser and T. Blu, "Approximation Error for Quasiinterpolators and (Multi) Wavelet Expansions," *Appl. Comput. Harmon. Anal.*, vol. 6, no. 2, pp, March 1999.

[13] G. Strang and G. Fix, "A Fourier Analysis of The Finite Element Variationall Method,"*in Constructive Aspects of Functional Analysis, G. Geymonat, Ed, Rome: Edizioni Cremonese*, 1973.

[14] R.C. Gonzalez, *Digital Image Processing*. New Jersey: Prentice Hall, 2002.

[15] L. Shin, H.W. Park, and Y. Piao, "Image Resolution Enhancement Using Inter-subband Correlation in Wavelet Domain," *Int. Conf. Image Proces.*, vol. 1, 2007.

[16] D. B. Chuang, S.S. Hemami, and W.K. Carey, "Regularity-Preserving Image Interpolation," *IEEE Transaction on Image Processing*, vol. 8, no. 9, September 1999.

[17] G. Anbarjafari and H. Demirel, "Image Super Resolution Based on Interpolation of Wavelet Domain High Frequency Subbands and The Spatial Domain Input Image," *ETRI Journal*, vol. 32, no. 3, june 2010.

[18] S. Mallet, *A Wavelet Tour of Signal Processing*. New York: Academic: 2nd ed, 1999.

[19] G. Peyre, Matlab Implementation of Wavelet Transforms. [Online]. https://www.ceremade.dauphine.fr/~peyre/numerical-tour/

[20] I. Daubechies, *Ten Lectures on Wavelets*. New York: SIAM, 1992.